

A non-cytotoxic dendrimer with innate and potent anticancer and anti-metastatic activities

Shiqun Shao¹, Quan Zhou¹, Jingxing Si^{1,2}, Jianbin Tang¹, Xiangrui Liu¹, Meng Wang³, Jianqing Gao³, Kai Wang², Rongzhen Xu² and Youqing Shen^{1*}

The structural perfection and multivalency of dendrimers have made them useful for biodelivery and bioactivity via peripheral functionalization and the modulation of core-forming structures and dendrimer generations. Yet only few dendrimers have shown inherent therapeutic activity arising from their inner repeating units. Here, we report the synthesis and characterization of a polyacylthiourea dendrimer with inherent potent anticancer activity and the absence of cytotoxicity in mice. The poly(ethylene glycol)-functionalized fourth generation of the dendrimer, which can be efficiently synthesized from sequential click reactions of orthogonal monomers, displays low in vivo acute and subacute toxicities yet potently inhibits tumour growth and metastasis. The dendrimer's in vivo anticancer activity arises from the depletion of bioavailable copper and the subsequent inhibition of angiogenesis and cellular proliferation. When compared with some clinically used cytotoxin drugs, the dendrimer exerts inherent anticancer activity via non-cytotoxic pathways and leads to higher therapeutic efficacy, yet without cytotoxin-induced side effects.

Synthetic polymers used in medicine, such as poly(ethylene glycol) (PEG), generally have no therapeutic activities but are used as excipients^{1–3}. In recent decades, polymers have been increasingly employed as nanocarriers to encapsulate or conjugate anti-tumour agents, including protein drugs such as neocarzinostatin, small-molecule chemotherapeutic drugs such as doxorubicin, and nucleic acid drugs such as DNA and small interfering RNA (siRNA), to fabricate various nanomedicines, in order to improve their pharmacokinetics and tumour accumulation, and thereby reduce adverse effects of drugs and increase their therapeutic efficacy^{2,4,5}.

Recently, a few synthetic polymers have been found to have some intrinsic pharmaceutical activities^{6,7}. For instance, poloxamers are shown to inhibit the activity of adenosine triphosphate-binding cassette pumps in multidrug resistant (MDR) tumours⁸. Dendrimers, the highly branched three-dimensional macromolecules with precise molecular structures⁹, have been endowed with bioactivities mainly from their surface functionalities^{10–12}. For instance, dendrimers with amine or hydroxyl surfaces¹³ and dendritic polyglycerol sulfates¹⁴ or dendrimer-like PEG glycopolymers¹⁵ were found to have anti-inflammatory activity by inhibiting related enzymes, whereas azabisphosphonate-capped dendrimers directed monocytes towards anti-inflammatory activation and exerted therapeutic effects against rheumatoid arthritis^{16,17}. Vivagel (SPL7013 gel), with a naphthalene disulfonate-terminated poly-L-lysine (PLL) dendrimer as the active ingredient, has potent human immunodeficiency virus-1 and herpes simplex virus-2 inhibitory activity¹⁸ and is currently in clinical trial phase III. Furthermore, highly cationic polypropylene imine (PPI) and PLL dendrimers with an amine surface showed some in vivo anticancer and anti-angiogenesis activities^{19,20}. However, given that these polymers have some intrinsic (that is, functioning without active pharmaceutical ingredients) therapeutic activities^{19–22}, none is yet sufficiently potent as an anticancer drug.

Exemplified by natural therapeutic polymers such as antibodies^{23,24}, polymers are particularly advantageous as macromolecular drugs²⁵ in their nanoscale hydrodynamic sizes and multivalence, which may render them long blood-circulation times^{1–3} and tumour accumulation²⁶ as well as high selectivity and activity^{27–29}. Here, we present a readily built polyacylthiourea dendrimer that per se can efficiently inhibit the growth of various tumours including MDR tumours, and even efficiently inhibit tumour metastasis. More significantly, in contrast to cytotoxin-based anticancer drugs that cause adverse effects due to unintended intoxication of healthy cells, this dendrimer can be considered non-cytotoxic and has low acute and subacute in vivo toxicities with an intravenous (i.v.) median lethal dose (LD₅₀) greater than 1 g kg⁻¹ in mice, and thus causes almost no noticeable adverse effects during the treatments. The dendrimer is the first non-cytotoxic dendrimer of inherent and potent in vivo anticancer activity.

Results

Dendrimer synthesis and properties. Isothiocyanates (R-NCS) react with amines and produce thiourea moieties without byproducts. The reaction is highly efficient without need of catalyst and insensitive to oxygen and water, meeting all the criteria of click chemistry³⁰. It has been extensively used in various bioconjugations and even dendron ligation³¹. The thiol/methacrylate-based Michael addition reaction is another proven click reaction³². Accordingly, two orthogonal monomer pairs—2,2-bis(methacryloyloxymethyl)propionyl isothiocyanate (BMAITC)/cysteamine (CA) and 2,2-bis(methacryloyloxymethyl)ethyl isothiocyanate (BMITEC)/CA—were prepared to construct polyacylthiourea (PATU) and polythiourea (PTU) dendrimers, respectively, as illustrated in Fig. 1 and Supplementary Scheme 1.

Tris(2-aminoethyl)amine, as the core-forming compound, reacted with a slight excess of BMAITC (BMAITC/NH₂ = 1.1) and produced the first-generation (G1) PATU dendrimer with three

¹Center for Bionanoengineering and Key Laboratory of Biomass Chemical Engineering of Ministry of Education, College of Chemical and Biological Engineering, Zhejiang University, 310027 Hangzhou, China. ²The Second Affiliated Hospital of School of Medicine, Zhejiang University, 310009 Hangzhou, China. ³College of Pharmaceutical Science, Zhejiang University, 310058 Hangzhou, China. Shiqun Shao and Quan Zhou contributed equally to this work. *e-mail: shenyq@zju.edu.cn

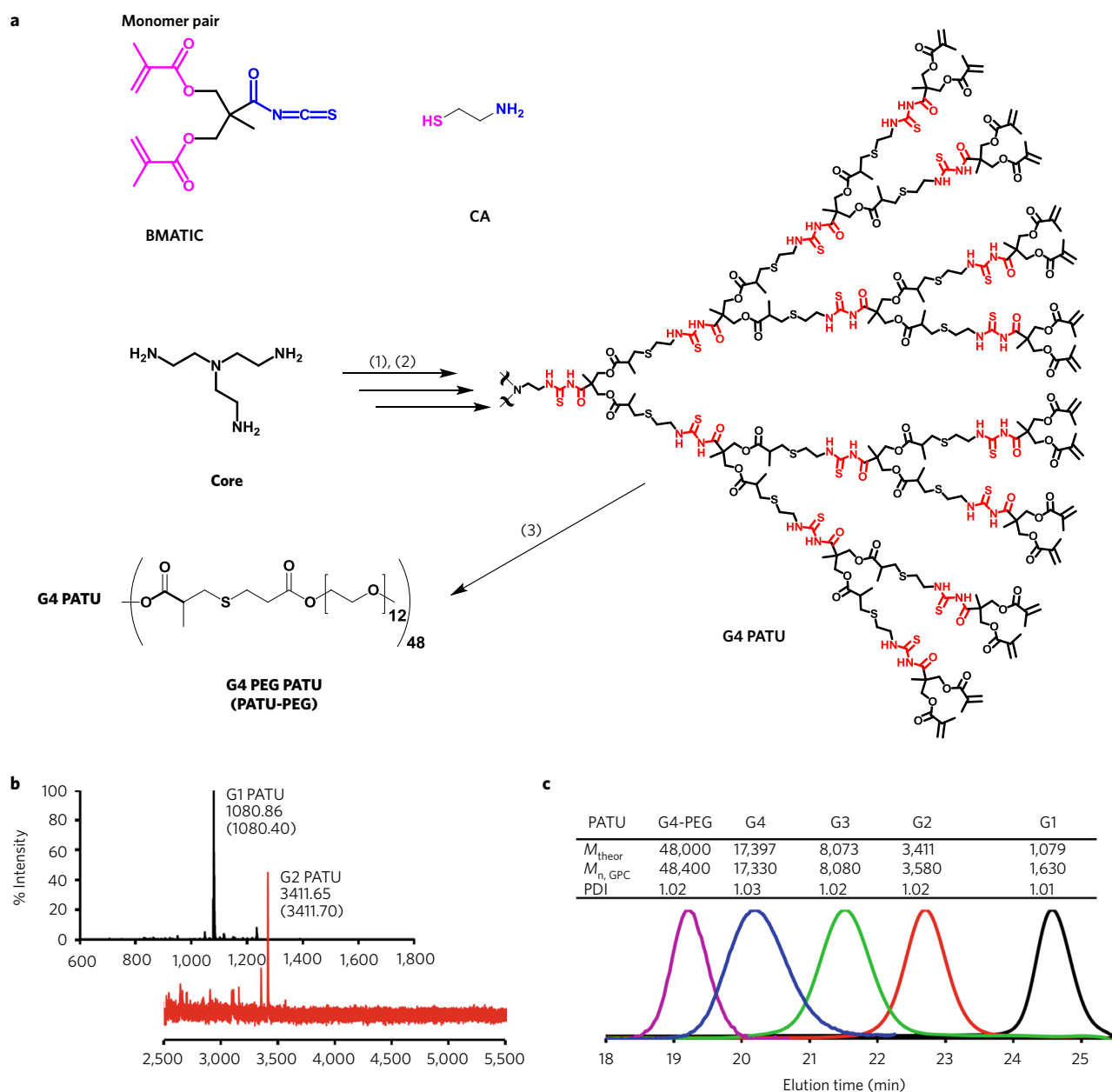


Fig. 1 | Facile synthesis and characterizations of PATU dendrimers. a, Synthesis of PATU dendrimers from BMAITC and CA. Only one dendron is shown. Reactions required are numbered as (1), (2) and (3); the PEGylated G4 PATU dendrimer is abbreviated as PATU-PEG. **b**, MALDI-TOF-MS spectra of the G1 and G2 PATU dendrimers with their calculated $[M + H]^+$ values in parentheses. **c**, Molecular weights of the PATU dendrimers calculated from the structure (M_{theor}), or measured by GPC ($M_{n, \text{GPC}}$, number-averaged) and the polydispersity index (PDI).

acylthiourea groups and six methacrylate termini. The reaction finished in less than 3 h at room temperature and the resulting G1 PATU dendrimer was easily isolated by precipitation in hexane in a 95% yield. The matrix-assisted laser-desorption ionization time-of-flight mass spectrometry (MALDI-TOF MS) spectrum confirmed its molecular precision (molecular weight: 1,079.40; Fig. 1b). The methacrylate termini of the G1 dendrimer then reacted with a slight excess of CA (1.05 equiv. to methacrylate group) in dimethyl sulfoxide (DMSO) for 30 min at room temperature. After removal of the excess CA by simply washing with brine solution, the amine-terminated molecule (G1.5 PATU) was obtained. Repetition of these two steps produced dendrimers of desirable generations (Fig. 1a).

The molecular weights of these PATU dendrimers were initially determined using MALDI-TOF MS spectra, but only the first and second generations gave their molecular signals (Fig. 1b).

The molecular signals of higher generations did not appear in the spectra because their copious thiourea groups prevented them from ionizing³³. Gel permeation chromatography (GPC) equipped with an 18-channel laser light scattering detector was used for determining their molecular weights, which all agreed well with their calculated values (Fig. 1c), and their polydispersities were all very close to a unit, suggesting their structural perfection as gauged by NMR spectra (Supplementary Figs. 1–5). The characteristic peaks of the resulting acylthiourea groups were observed in the Fourier transform infrared spectrum at 3,445 (N–H), 1638 (HN–C=O), 1,514 (N–H) and 1,090 (C=S) cm^{-1} (Supplementary Fig. 6a).

The PATU dendrimers with methacrylate termini were water-insoluble. Thus, short PEG chains (PEG550) were introduced to the periphery of the G4 dendrimer by the thiol/methacrylate reaction, affording the PEGylated G4 PATU dendrimer (PATU-PEG;

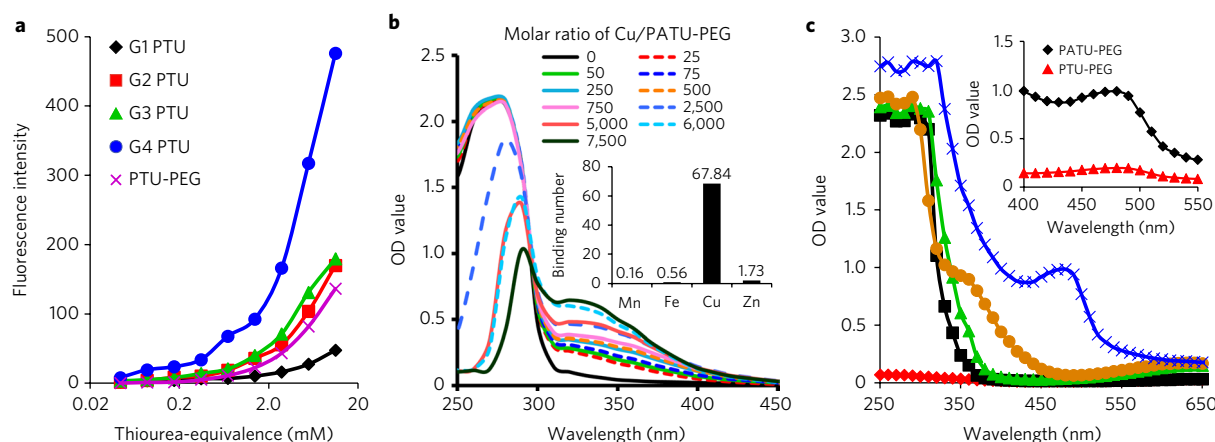


Fig. 2 | Autofluorescence and copper-chelation capability of the dendrimers. **a**, Generation-dependent fluorescence intensity at 430 nm of PTU dendrimers at various thiourea-equivalent concentrations in DMF on excitation at 366 nm. **b**, Ultraviolet–visible absorbance spectra of PATU-PEG (10 μM) solutions with different amounts of CuCl_2 added after subtracting the spectra of uncomplexed CuCl_2 in the solution. The inset shows the copper selectivity of PATU-PEG over other microelement ions in terms of the number of ions complexed per PATU-PEG molecule. PATU-PEG (20 μM) was added into an aqueous solution containing 20 mM each of the metal ions (Mn^{2+} , Fe^{2+} , Cu^{2+} and Zn^{2+}). **c**, Reduction of Cu^{2+} to Cu^+ by PATU-PEG detected by bathocuproine disulfonate (BCS). Ultraviolet–visible absorbance spectra of Tris-HCl (10 mM, pH 7.5) solutions containing the following components, respectively: BCS (red), BCS + PATU-PEG (black), BCS + Cu^{2+} (green), PATU-PEG + Cu^{2+} (orange) and PATU-PEG + Cu^{2+} + BCS (blue). The inset compares the absorbance of the Cu^+ -BCS complex formed in the PATU-PEG/ Cu^{2+} -BCS solution with that in the PTU-PEG/ Cu^{2+} -BCS solution (25 $^\circ\text{C}$; 270 μM BCS, 2.5 μM Cu^{2+} , 10 μM PATU-PEG or PTU-PEG).

Fig. 1a). The ^1H NMR and ^{13}C NMR spectra showed a complete addition of PEG chains (Supplementary Figs. 7 and 8). The PATU-PEG had a molecular weight matching its theoretical value with a low polydispersity (Fig. 1c). Following the same procedures, the PEGylated low-generations of PATU dendrimers (that is, G1-PEG, G2-PEG and G3-PEG PATU dendrimers) were also prepared and then characterized by ^1H NMR, ^{13}C NMR and GPC (Supplementary Figs. 11–13).

Similarly, the BMITC/CA monomer pair was used to construct PTU dendrimers with the same chemical structures as PATU except for the absence of the acyl groups adjacent to the thiourea moieties (Supplementary Scheme 1). All the reaction conditions were the same and the subsequent characterizations using various techniques demonstrated the structural perfection of PTU dendrimers (Supplementary Information and Supplementary Figs. 6b, 14–21 and 22a).

It should be pointed out that the synthesis of both dendrimers was extremely efficient—the growth of one generation, including the reactions, purification and isolation, could be completed within 4 h with an overall yield higher than 90%, and it took less than 24 h to obtain grams of G4 dendrimers in our lab.

Very unexpectedly, the subtle structural difference between PATU and PTU dendrimers caused dramatic differences in their properties, one of which is that the PTU dendrimers were fluorescent at 430 nm on excitation at 366 nm (Fig. 2a) even though the thiourea moiety is not a conventional fluorophore, whereas PATU dendrimers had no fluorescence. Polyamidoamine and PPI dendrimers were found to have inherent fluorescence, which was ascribed to the oxidative impurities produced during the synthesis and storage³⁴. We thus examined whether the PTU fluorescence was induced by oxidation. Bubbling oxygen gas into the dendrimer solutions did boost the fluorescence intensity of G3 polyamidoamine dendrimer but did not affect those of G3 PTU and PTU-PEG dendrimers (Supplementary Fig. 23), indicating that the PTU fluorescence might not come from oxidative impurities. The fluorescence of PTU-PEG may arise from the aggregation-induced emission^{35,36}; that is, the unpaired electrons of the nitrogen and sulfur heteroatoms in close proximity in the dendrimer form so-called spatially conjugated heterodox clusters that serve as fluorophores³⁷.

Interestingly, both dendrimers exhibited strong but different copper-chelation capabilities. On addition of Cu^{2+} ions into the PATU-PEG aqueous solution, the absorption peak at 270 nm of acylthiourea shifted gradually and disappeared at high Cu^{2+} concentrations, while a shoulder appeared at approximately 320–350 nm (Fig. 2b). The binding constant and binding number were determined by isothermal titration calorimetry experiments to be $(2.7 \pm 0.3) \times 10^5 \text{ M}^{-1}$ and 84.5, respectively (Supplementary Fig. 24a). The binding number was further validated by directly determining the copper/dendrimer molar ratio in the purified PATU-PEG/ Cu complex, which was 76.8 ± 10.0 . After complexing so many copper ions, the hydrodynamic diameter of PATU-PEG increased from about 3 nm to about 10 nm as measured by dynamic laser light scattering (Supplementary Fig. 24b). Transmission electron microscopy images showed that copper complexation induced not only the size growth of the individual dendrimer molecules but also their aggregation (Supplementary Fig. 25). In addition, PATU-PEG selectively bound Cu^{2+} ions over other common microelement ions (Fig. 2b, inset and Supplementary Fig. 24c). In the case of PTU-PEG, addition of Cu^{2+} into the PTU-PEG solution gradually quenched its intrinsic fluorescence (Supplementary Fig. 22b) due to copper ion-caused quenching³⁸. The Cu^{2+} complexation also made the thiourea absorption peak at 250 nm disappear and a plateau emerge at 270–290 nm (Supplementary Fig. 22c). Among the tested ions, only Cu^{2+} efficiently quenched the PTU-PEG fluorescence, suggesting the highly selectively binding of PTU-PEG to Cu^{2+} over other metal ions (Supplementary Fig. 22d).

The complexation between acylthiourea/thiourea and CuCl_2 involves the reduction of Cu^{2+} to Cu^+ by the moieties³⁹. The formed Cu^+ was detected by bathocuproine disulfonate (BCS), a Cu^+ -specific sequestering agent⁴⁰. On addition of BCS to the PATU-PEG/ CuCl_2 or PTU-PEG/ CuCl_2 solution, a characteristic peak of the Cu^+ -BCS complex appeared at 480 nm (Fig. 2c and Supplementary Fig. 22e), confirming the Cu^+ formation⁴⁰. The intensity of the Cu^+ -BCS complex in the PATU-PEG/ Cu^{2+} solution was much higher than that in the PTU-PEG/ Cu^{2+} solution (Fig. 2c, inset), suggesting a stronger reducing ability of the PATU dendrimers. The X-ray photoelectron spectroscopy measurements

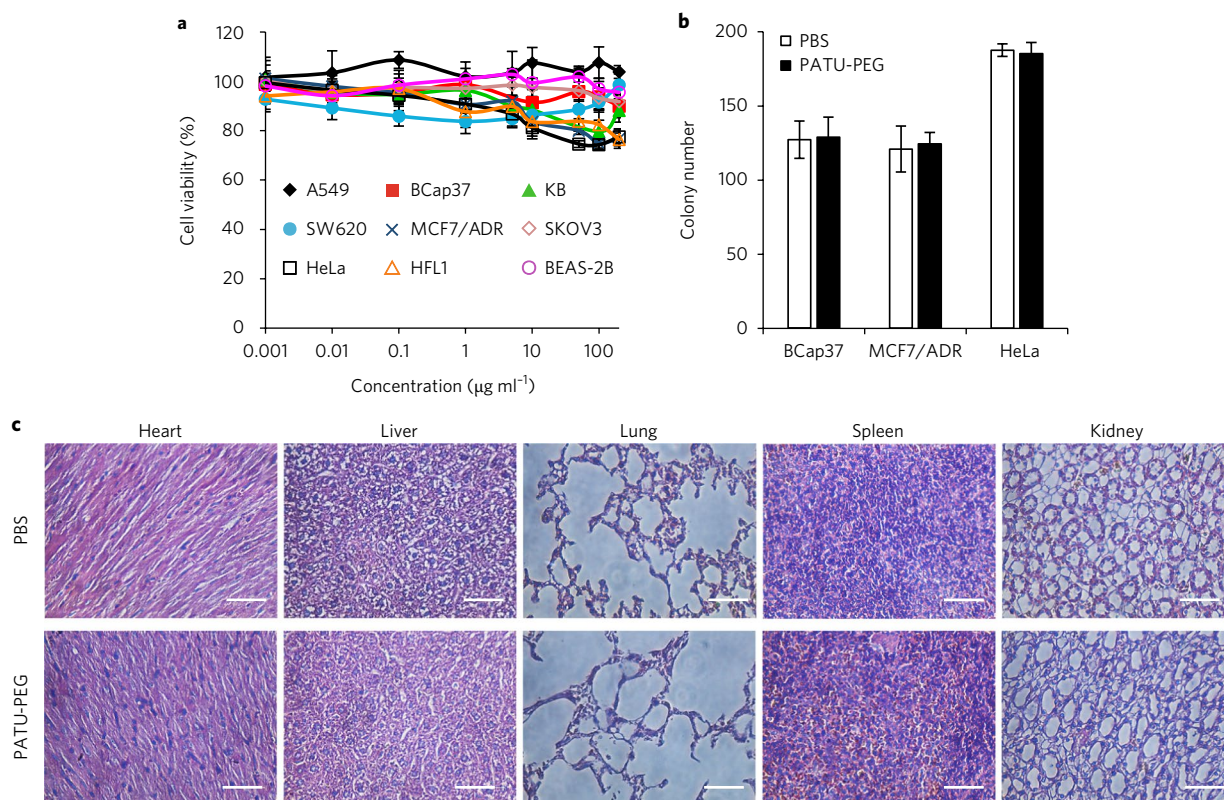


Fig. 3 | Assays of in vitro cytotoxicity and in vivo toxicity of PATU-PEG. **a**, The MTT assay of PATU-PEG for different cell lines (48 h treatment). **b**, Comparison of colony formation of cells with or without PATU-PEG (200 µg ml⁻¹) treatment. Cells were seeded in six-well plates and cultured for 10 d. Colonies containing more than 50 cells were counted. **c**, Representative H&E staining images of major organs from the control and PATU-PEG-treated mice (250.0 mg kg⁻¹ given once). Animals were killed at 24 h post injection. Scale bars, 50 µm. All data are expressed as mean ± s.d.

showed that 45% of copper ions in PATU-PEG/CuCl₂ were in the Cu⁺ state and the rest were in the Cu²⁺ state. However, only 4% of copper in PATU-PEG/CuCl₂ existed as Cu⁺ ions (Supplementary Fig. 26), indicating that the thiourea moieties in PATU could not effectively reduce Cu²⁺.

The dendrimers exhibit low acute and subacute in vivo toxicity. The in vitro and in vivo toxicity of PATU-PEG and PTU-PEG were assessed with an emphasis on PATU-PEG due to its better anticancer activity, which is shown later. In the 3-(4,5-dimethylthiazol-2-yl)-2,5-diphenyltetrazolium bromide (MTT) assay (Fig. 3a and Supplementary Fig. 27), even at concentrations as high as 200 µg ml⁻¹, neither PATU-PEG nor PTU-PEG significantly inhibited the cell growth of various human tumour cell lines (A549, BCap37, KB, SW620, SKOV3, MCF7/ADR and HeLa) and non-tumourigenic cell lines (HFL1 and BEAS-2B). Similarly, the PEGylated low-generation PATU dendrimers also demonstrated low in vitro cytotoxicity against human tumour cell lines (SW620, MCF7/ADR) and a non-tumourigenic cell line (BEAS-2B) (Supplementary Fig. 28). PATU-PEG also had no effect on the cell proliferation or colony-forming ability (Fig. 3b and Supplementary Fig. 29), cellular morphologies (Supplementary Fig. 30) and cell cycle (Supplementary Fig. 31).

Acute-toxicity tests revealed that the values of the i.v. LD₅₀ and 95% confidence interval for PATU-PEG in imprinting control region (ICR) mice were 1,176 mg kg⁻¹ and 1,050–1,317 mg kg⁻¹, respectively (values for dose (mg kg⁻¹) (number of dead/tested mice): 1,914.1 (10/10), 1,531.3 (8/10), 1,225.0 (7/10), 980.0 (2/10) and 784.0 (0/10)). Histological analysis of major organs of the mice treated with PATU-PEG showed no obvious damage or lesions

(Fig. 3c). PATU-PEG treatments for five consecutive days caused no significant changes in mouse serum chemistry, including liver and renal functions and myocardial enzymogram (Table 1). Therefore, the dendrimers, particularly PATU-PEG, can be considered non-cytotoxic and to have low in vivo acute and subacute toxicity.

PATU-PEG efficiently inhibits the growth of multiple human xenograft tumours. The anticancer activities of the dendrimers were first tested using athymic nude mice bearing BCap37 breast tumours at a dendrimer dose of 1.0 µmol kg⁻¹ (50 mg kg⁻¹ PATU-PEG or 48.6 mg kg⁻¹ PTU-PEG). The body weights of animals in each group remained steady, indicating that they did not cause severe systemic toxicity (Supplementary Fig. 32a). Unexpectedly, both the non-cytotoxic PATU-PEG and PTU-PEG effectively inhibited the tumour growth, particularly PATU-PEG (Fig. 4a and Supplementary Figs. 32b and 33a). Indeed, immunohistochemical analysis of these tumours further revealed that PATU-PEG more significantly downregulated vascular endothelial growth factor (VEGF) expression, decreased the microvessel number (cluster of differentiation 31 (CD31) staining) and arrested cellular proliferation (antigen Ki-67 staining) than PTU-PEG (Supplementary Fig. 32c–f). Considering their similar chemical structures, these results indicate that the acylthiourea groups play an important role in the anticancer activity. Furthermore, these dendrimers without conventional therapeutic moieties showed potent anticancer activity, representing a new type of synthetic polymers of intrinsic anticancer activity.

The intrinsic anticancer activity of PATU-PEG was further confirmed and assessed using Doxil as a positive control. In nude mice bearing BCap37 tumours (Fig. 4b), PATU-PEG (50 mg kg⁻¹) inhibited tumour growth as effectively as Doxil at a dose of 4 mg kg⁻¹.

Table 1 | Serum chemistry of mice treated with PBS or PATU-PEG^a

ICR mice (n = 10)	PBS	PATU-PEG (50 mg kg ⁻¹)	PATU-PEG (100 mg kg ⁻¹)	ANOVA P-levels ^b
ALT (U l ⁻¹)	48.7 ± 2.5	50.3 ± 3.1	49.3 ± 3.8	0.82
CK (U l ⁻¹)	626.3 ± 105.6	884.0 ± 63.9	820.6 ± 142.9	0.06
CKMB (U l ⁻¹)	449.3 ± 93.0	620.3 ± 53.5	582.6 ± 122.1	0.14
AST (U l ⁻¹)	80.0 ± 4.0	88.3 ± 6.4	90.6 ± 9.1	0.21
LDH (U l ⁻¹)	460.7 ± 310.0	409.0 ± 90.9	350.3 ± 38.5	0.16
UREA (mM)	7.5 ± 0.8	7.3 ± 1.3	7.4 ± 0.4	0.94
CREA (µM)	21.8 ± 4.2	16.2 ± 1.6	17.4 ± 2.1	0.11

Data are mean ± s.d. ALT, alanine transaminase; CK, creatine kinase; CKMB, creatine kinase mb isoenzyme; AST, aspartate transaminase; LDH, lactate dehydrogenase; UREA, blood urea nitrogen; CREA, creatinine; ANOVA, analysis of variance. ^aMice were intravenously treated daily for 5 days with PBS or PATU-PEG (50 mg kg⁻¹ or 100 mg kg⁻¹). Blood samples were collected for serum chemistry analysis one day after the fifth treatment. ^bAll Tukey post-hoc comparison, P-levels > 0.05.

However, whereas the animals treated with Doxil were found listless and losing weight on administration (Supplementary Fig. 34), those treated with PATU-PEG had no observable change in behaviours and general health, and their average body weight increased steadily throughout the study (Supplementary Fig. 34). This correlated well with its low toxicity observed above. These data also indicate that PATU-PEG was well tolerated by animals but exerted comparable anticancer activity to the established first-line anticancer drug Doxil, much more potent than the reported cationic PLL dendrimer²⁰.

To examine whether the anticancer effect of PATU-PEG originates from its copper-chelation property, the effects of Cu²⁺ and Cu⁺ on the cytotoxicity of PATU-PEG were first investigated. Compared with the non-toxicity of PATU-PEG, the PATU-PEG/Cu²⁺ complex had the same cytotoxicity as Cu²⁺ whereas PATU-PEG/Cu⁺ was less toxic than CuCl itself (Supplementary Figs. 35 and 36a), but the half maximal inhibitory concentration (IC₅₀) values of both complexes were still higher than 100 µg ml⁻¹, indicating that unlike the copper ligand-grafted phosphorus dendrimers⁴¹, PATU-PEG does not exert anticancer activity via the cytotoxicity of its copper complex. Subsequently, the *in vivo* tumour inhibition efficacies of partially or fully Cu²⁺-complexed PATU-PEG were compared with that of copper-free PATU-PEG to infer the influence of copper complexing on the anticancer activities. According to the maximal binding number of copper per dendrimer molecule measured above, PATU-PEG (50 mg kg⁻¹) was pre-complexed with 3.2 mg kg⁻¹ Cu²⁺-equiv. (Concentration_{PATU-PEG}/Concentration_{Cu} molar ratio = 1/48) to make the PATU-PEG complex with copper at its 50% capacity (denoted as PATU-PEG/0.5Cu²⁺). Similarly, the fully copper-saturated PATU-PEG (PATU-PEG/Cu²⁺) was obtained by mixing 50 mg kg⁻¹ PATU-PEG with 6.4 mg kg⁻¹ Cu²⁺-equiv. (Concentration_{PATU-PEG}/Concentration_{Cu(II)} = 1/96). They were used to treat BCap37 tumour-bearing nude mice and compared with copper-free PATU-PEG (Fig. 4c,d). The copper-free PATU-PEG significantly suppressed tumour growth compared with the control and its copper complexes (Fig. 4c and Supplementary Figs. 33b and 36d). PATU-PEG-treated tumours resected after the animals were killed had significantly decreased VEGF expression, microvessel count and Ki-67 positive staining (Fig. 4d and Supplementary Fig. 36f–h), and many more apoptotic cells, as detected by the terminal deoxynucleotidyl transferase-mediated dUTP nick end labelling (TUNEL) assay (Fig. 4d). The reduction in VEGF and Ki-67 by PATU-PEG was further validated in tumour-bearing mice after a single high-dose treatment (250 mg kg⁻¹; Supplementary Fig. 37). Consequently, pre-complexation of copper mitigated PATU-PEG's antitumour activity (Fig. 4c and Supplementary Figs. 33b and 36d). For comparison, CuCl₂ alone at a 3.2 mg kg⁻¹ Cu²⁺-equiv. dose showed no tumour inhibitory effect (Supplementary Fig. 38). A higher dose of CuCl₂ at 6.4 mg kg⁻¹ Cu²⁺-equiv. was highly toxic, resulting in significant

mortality (Supplementary Fig. 38c). These comparisons demonstrate a positive correlation between the tumour inhibitory activity of PATU-PEG and its copper-binding capacity.

The anticancer activity of PATU-PEG was further validated using ammonium tetrathiomolybdate (TM), a strong copper-depleting agent for cancer treatment under clinical trials⁴², as a positive control. TM is mostly administered orally (25–50 mg kg⁻¹ in mice), and no pharmacokinetic data in mice are available yet. Thus, an *i.v.* dose titration was performed and showed that the *i.v.* injection of TM at a dose of 2 mg kg⁻¹ or 10 mg kg⁻¹ produced a similar ceruloplasmin (Cp) lowering profile in mice to that produced by 50 mg kg⁻¹ of PATU-PEG (shown later in Fig. 7d). The tumour inhibition activity of PATU-PEG (50 mg kg⁻¹) was thus evaluated with TM at both doses as the control. PATU-PEG more effectively inhibited the growth of BCap37 tumours (Fig. 4e and Supplementary Figs. 33c and 39b) and SW620 colon tumours (Fig. 4f and Supplementary Figs. 33d and 40b) than TM. Furthermore, a higher dose of PATU-PEG at 100 mg kg⁻¹ gave even greater tumour inhibition (Supplementary Fig. 40d,f), indicating that PATU-PEG's anticancer activity was dose dependent. In all the experiments, no PATU-PEG-treated animals showed toxicity complications (Supplementary Figs. 39a and 40a,e).

The human adriamycin-resistant MCF-7/ADR tumour model was used to further evaluate PATU-PEG's anticancer activity against MDR tumours and its combination with the first-line clinical anticancer drug doxorubicin (DOX). The *in vitro* MTT assay shows that the combination of DOX with PATU-PEG did not enhance its cytotoxicity to MCF7/ADR cells (Supplementary Fig. 41a). As shown in Fig. 4g, DOX (4 mg kg⁻¹) only slightly inhibited the growth of the drug-resistant tumours, as found in the literature⁴³, whereas PATU-PEG effectively suppressed tumour growth *per se*. The combination of PATU-PEG (50 mg kg⁻¹) with DOX (4 mg kg⁻¹) did not significantly increase the tumour inhibitory effect compared with PATU-PEG alone (Fig. 4g and Supplementary Figs. 33e and 41c). However, more frequent dosing of PATU-PEG (daily for 8 days) led to regression of the established MCF7/ADR tumour xenografts (Supplementary Fig. 41d–f); two of the eight animals had even complete tumour regression. These results indicate that PATU-PEG is not the substrate of multidrug resistance and thus can effectively inhibit the growth of MDR tumours, but it cannot reverse the multidrug resistance of MCF7/ADR.

PATU-PEG suppresses solid tumour metastasis and circulating tumour cell seeding. The anticancer efficacy of PATU-PEG and whether it can suppress tumour metastasis were further tested using an extremely aggressive and metastatic 4T1 murine mammary carcinoma model (Fig. 5), whose tumour growth and metastasis in BALB/c (albino, laboratory-bred strain) mice very closely mimic human breast cancer at stage IV⁴⁴. To track the metastatic tumour cells, the cells stably co-expressing luciferase and green

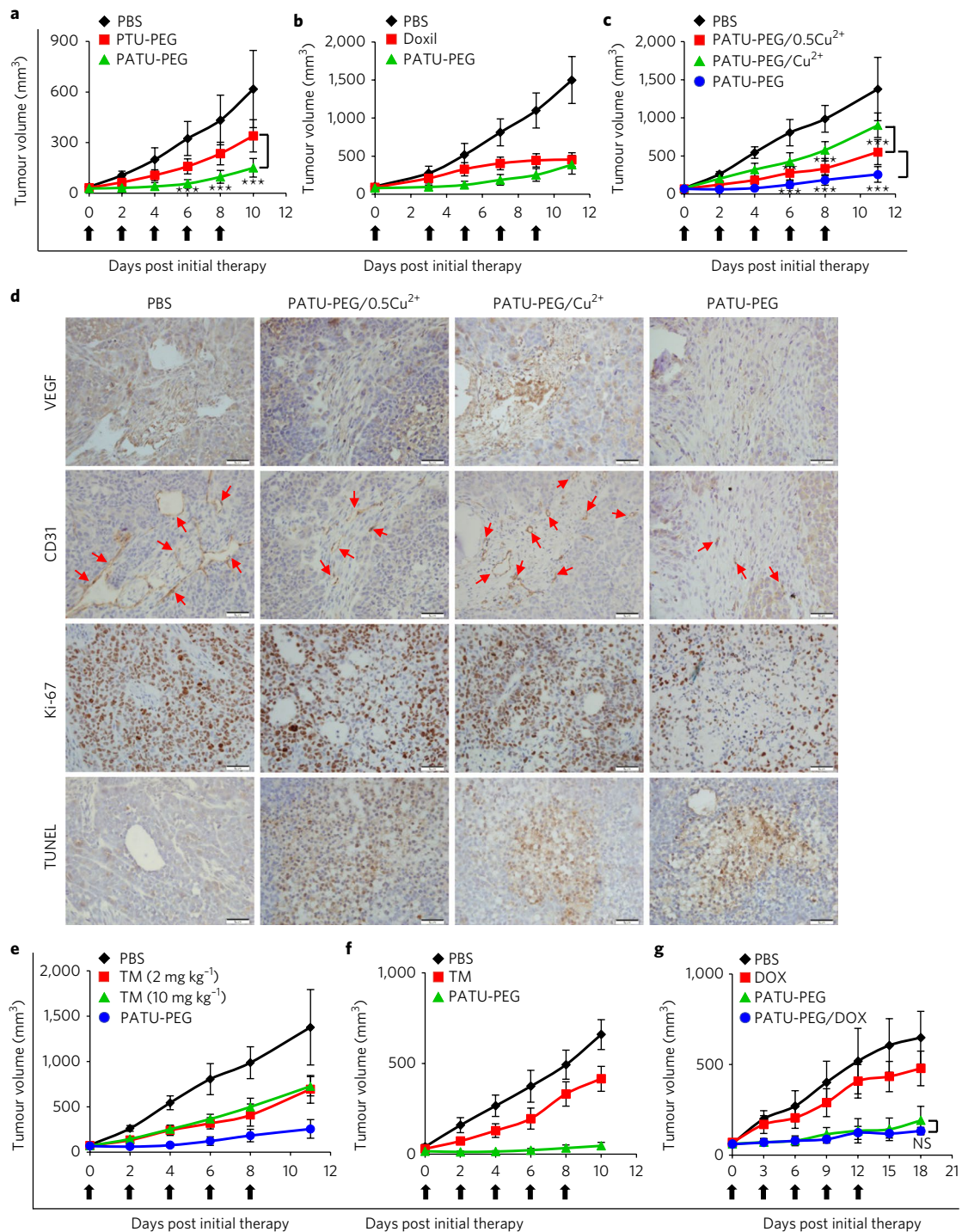


Fig. 4 | PATU-PEG inhibits the growth of multiple human tumours in vivo. **a**, Comparison between PATU-PEG and PTU-PEG in terms of anticancer efficacy. Nude mice bearing BCap37 tumours ($n=10$ per group) were intravenously injected with PBS, PATU-PEG ($1.0 \mu\text{mol kg}^{-1}$, 50 mg kg^{-1}) or PTU-PEG ($1.0 \mu\text{mol kg}^{-1}$, 48.6 mg kg^{-1}). **b**, Comparison of anticancer efficacy between PATU-PEG and Doxil. Nude mice bearing BCap37 tumours ($n=8$ per group) were intravenously injected with PBS, Doxil (4 mg kg^{-1} DOX-equiv.) or PATU-PEG (50 mg kg^{-1}). **c,d**, The effect of copper-binding on the anticancer activity of PATU-PEG. Nude mice bearing BCap37 tumours ($n=9$ per group) were intravenously injected with PBS, CuCl_2 (6.4 mg kg^{-1} Cu^{2+} -equiv.), PATU-PEG (50 mg kg^{-1}), PATU-PEG/ 0.5Cu^{2+} (50 mg kg^{-1} PATU-PEG pre-complexed with 3.2 mg kg^{-1} Cu^{2+} -equiv.) or PATU-PEG/ Cu^{2+} (50 mg kg^{-1} PATU-PEG pre-complexed with 6.4 mg kg^{-1} Cu^{2+} -equiv.). CuCl_2 treatments had no tumour inhibition but significant mortality at 6.4 mg kg^{-1} Cu^{2+} -equiv.. (Supplementary Figs. 36c and 38). **c**, Tumour volumes of mice as a function of time. **d**, Representative immunohistochemical staining of sections of tumour resected after the animals were killed. Red arrows, typical microvessels. Scale bars, $50 \mu\text{m}$. **e**, Tumour inhibitory effect of PATU-PEG against BCap37 tumours using TM as a positive control. Nude mice bearing BCap37 tumours ($n=9$ per group) were intravenously injected with PBS, TM (2 mg kg^{-1} or 10 mg kg^{-1}) or PATU-PEG (50 mg kg^{-1}). **f**, Tumour inhibition ability of PATU-PEG on SW620 tumours. Nude mice bearing SW620 tumours ($n=7$ per group) were intravenously injected with PBS, TM (2 mg kg^{-1}) or PATU-PEG (50 mg kg^{-1}). **g**, Tumour inhibition ability of PATU-PEG on MCF7/ADR tumours. Nude mice bearing MCF7/ADR tumours ($n=8$ per group) were intravenously injected with PBS, DOX (4 mg kg^{-1}), PATU-PEG (50 mg kg^{-1}) or PATU-PEG/DOX (50 mg kg^{-1} PATU-PEG, 4 mg kg^{-1} DOX). The dosing schedules are indicated by black arrows. All data are expressed as mean \pm s.d. $**P < 0.01$; $***P < 0.001$; NS, no significant difference.

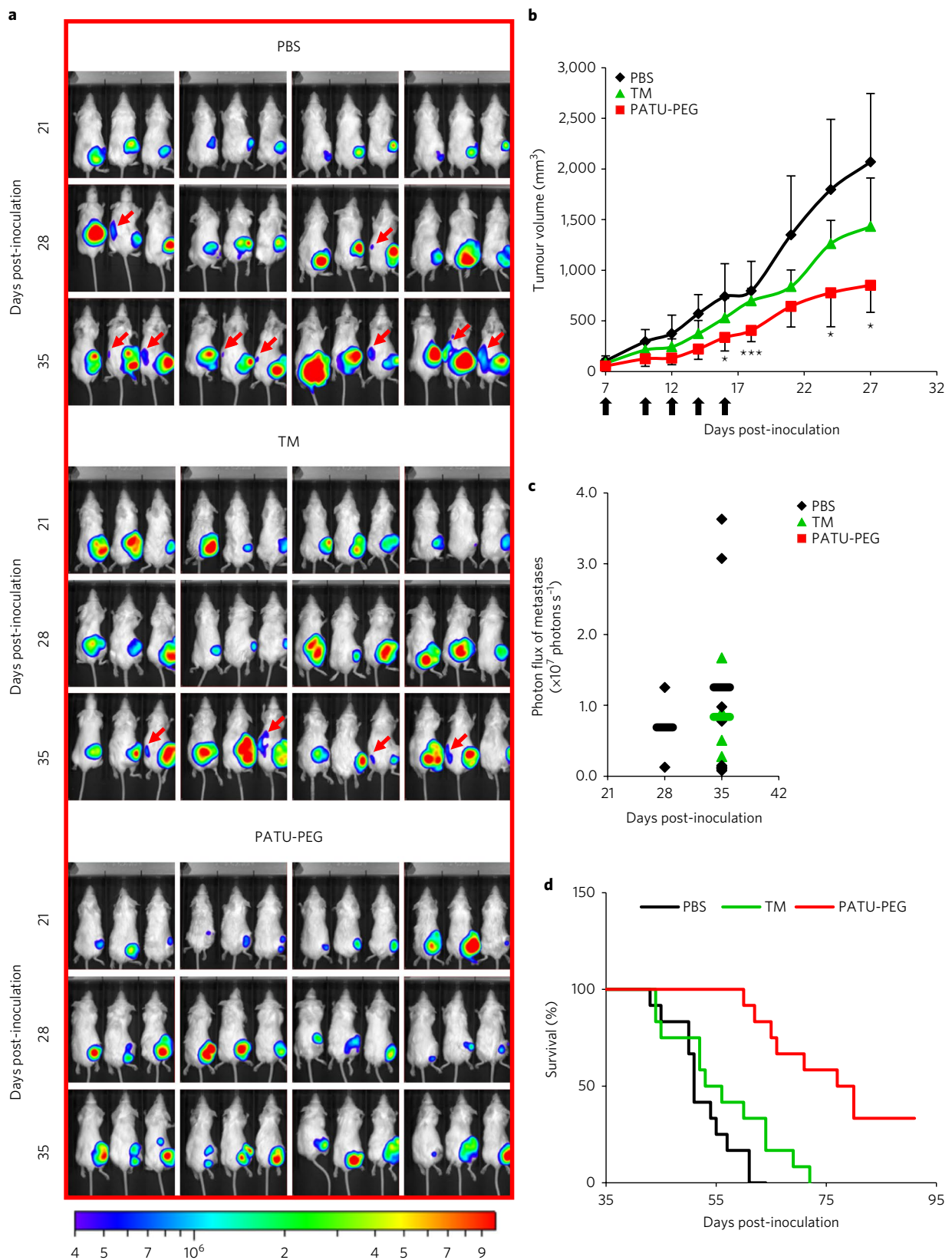


Fig. 5 | PATU-PEG inhibits spontaneous metastasis of primary breast tumours. 4T1-Luc-GFP cells (2×10^5 per mouse) were inoculated subcutaneously into the right hind legs of six- to eight-week-old syngeneic female BALB/c mice. On day 7 post tumour inoculation, the randomized mice ($n=12$ per group) were intravenously injected with PBS, TM (2 mg kg^{-1}) or PATU-PEG (50 mg kg^{-1}). **a**, Distant metastasis detected using in vivo bioluminescence imaging. Red arrows, metastatic foci. **b**, The primary tumour volumes of mice as a function of time. **c**, Intensity in each group measured from bioluminescence imaging. Bars, mean photon flux. The number of metastatic foci at 21, 28 and 35 days were, respectively, 0, 2 and 7 for PBS, 0, 0 and 4 for TM, and 0, 0 and 0 for PATU-PEG. **d**, Kaplan-Meier analysis of animals as treated above. Animals were killed when moribund, and the experiment was terminated on day 90. All data are expressed as mean \pm s.d. * $P < 0.05$; *** $P < 0.001$.

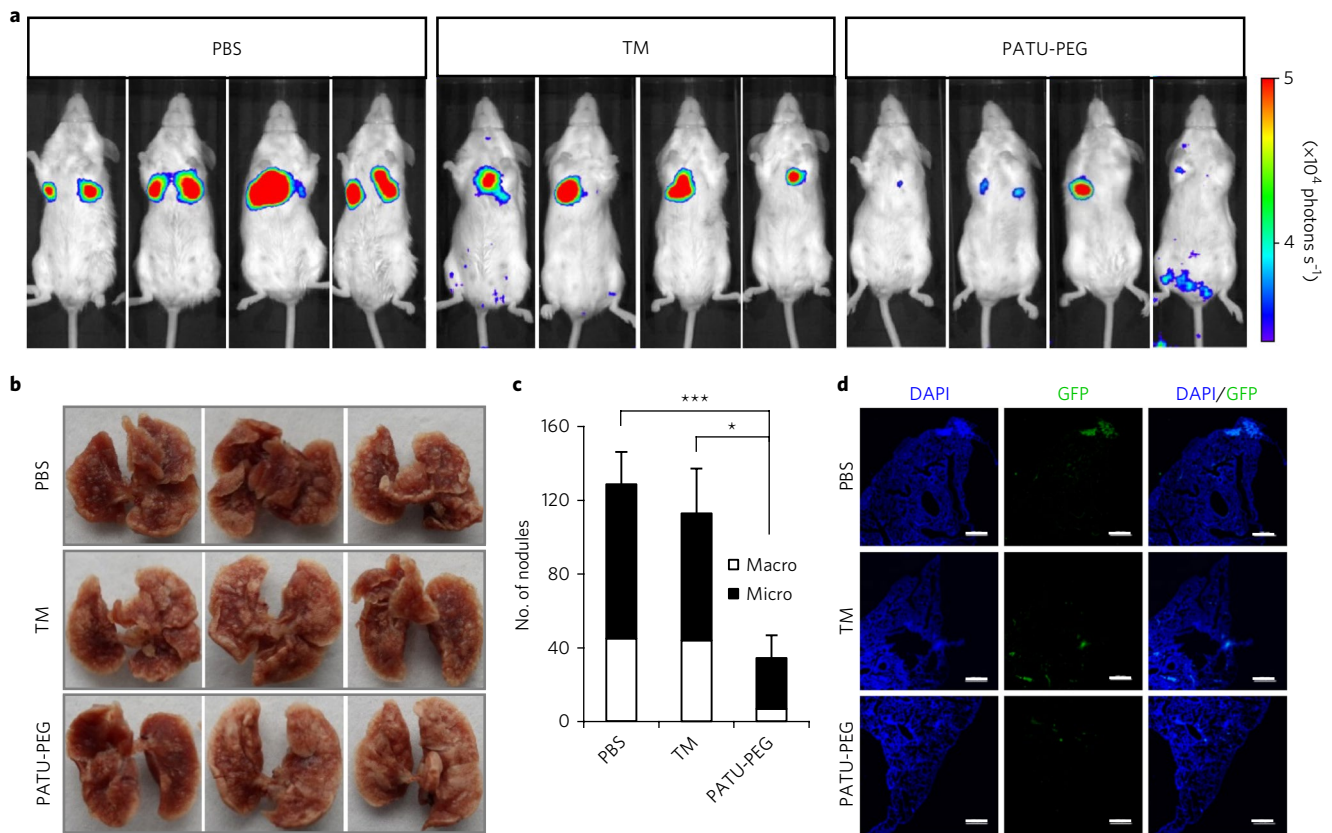


Fig. 6 | PATU-PEG suppresses lung seeding of tumour cells in circulation. 4T1-Luc-GFP cells (2×10^5 per mouse) were intravenously injected into six- to eight-week-old female BALB/c mice through the tail vein. On day 1 post-inoculation, i.v. treatment with PBS, TM (2 mg kg^{-1}) or PATU-PEG (50 mg kg^{-1}) was initiated (once every 2 days $\times 5$, $n = 10$ per group). Lung metastasis seeding was detected using bioluminescence imaging on day 10 post inoculation. **a**, Representative in vivo bioluminescent images of the lung metastasis seeding. **b**, Representative lungs resected on day 10. **c**, Visual counting of the average number of macro- and micro-metastases in the lung per mouse in each group. $n = 5$ per group. **d**, Representative images of the lung tissues stained with DAPI (blue) under fluorescent microscopy. The GFP of the 4T1-Luc-GFP tumours is excited and shown in green. All data are expressed as mean \pm s.d. * $P < 0.05$; *** $P < 0.001$.

fluorescent protein (4T1-Luc-GFP) were used. On day 7 post cell implantation, treatments with TM as the control were initiated and the tumour metastatic behaviour was monitored using in vivo bioluminescence imaging (Fig. 5a). Mice treated with PATU-PEG had a significantly slower tumour growth than those in the control and TM groups (Fig. 5b). In the control group of 12 mice, metastatic foci were observed in the left hind legs of two mice on day 28 and of seven mice on day 35. In the TM-treated group, 4 of the 12 mice were found to have metastatic foci on day 35, but no PATU-PEG-treated mice showed metastasis from the primary sites during the same observation period (Fig. 5a,c). As shown in the Kaplan–Meier plots for the time course of survival (Fig. 5d), the median survival times of the controlled and TM-treated animals were 52.4 and 56.3 d, respectively, and that of the PATU-PEG treated animals was longer than 77 d with one-third of them even alive at the end of the experiment on day 90.

It should be noted that pulmonary metastasis is commonly found in the wild 4T1⁴⁵ or 4T1-Luc⁴⁶ models. In our model, however, 4T1-Luc-GFP cells did not spread to lungs but to bones including crus bones and skulls (Supplementary Fig. 42c), consistent with the in vivo imaging (Fig. 5a).

We further tested the ability of PATU-PEG in suppressing tumour cell seeding mimicking circulating tumour cell metastasis to lungs. 4T1-Luc-GFP cells were intravenously injected through the tail vein into mice on day 0 as circulating tumour cells and the treatment was started one day later. Lung seeding of 4T1-Luc-GFP cells from the

circulation was observed in all the animals (Fig. 6a), but the mice treated with PATU-PEG had significantly fewer tumour foci than those in the control and TM groups (Fig. 6a,b and Supplementary Fig. 42e). Moreover, the percentage of macro-metastatic foci ($\geq 1 \text{ mm}$ in diameter) of all the tumour nodules in the lung in each group was 35% in the control, 39% in the TM group and 20% in the PATU-PEG group (Fig. 6c), indicating a stronger inhibition of PATU-PEG on the progression of micro-metastases ($< 1 \text{ mm}$ in diameter) to lethal macro-metastases⁴⁷. Histological fluorescence analysis of the resected lungs further confirmed the reduced tumour cell seeding in the PATU-PEG-treated mice (Fig. 6d).

Preliminary pharmacological study of PATU-PEG. PATU-PEG labelled with cyanine-7 (Cy7, a near-infrared fluorescent dye), Cy7-PATU-PEG, was used to investigate the in vivo plasma pharmacokinetics of PATU-PEG. After i.v. injection into the tumour bearing mice, Cy7-PATU-PEG had a relatively slow clearance from the blood with a blood retention of 21.5% of the injected dose at 1 h due to its macromolecular character (Fig. 7a). This result was further validated by technetium-99m (^{99m}Tc)-labelled PATU-PEG (^{99m}Tc-DTPA-PATU-PEG).

Cy7-PATU-PEG was also employed to study the in vivo bio-distribution behaviour of PATU-PEG in mice. As illustrated in Supplementary Fig. 43a, strong fluorescence emission was observed in the bladder at 30 min post injection. Considering PATU-PEG's hydrodynamic diameter of about 3 nm and the size threshold for

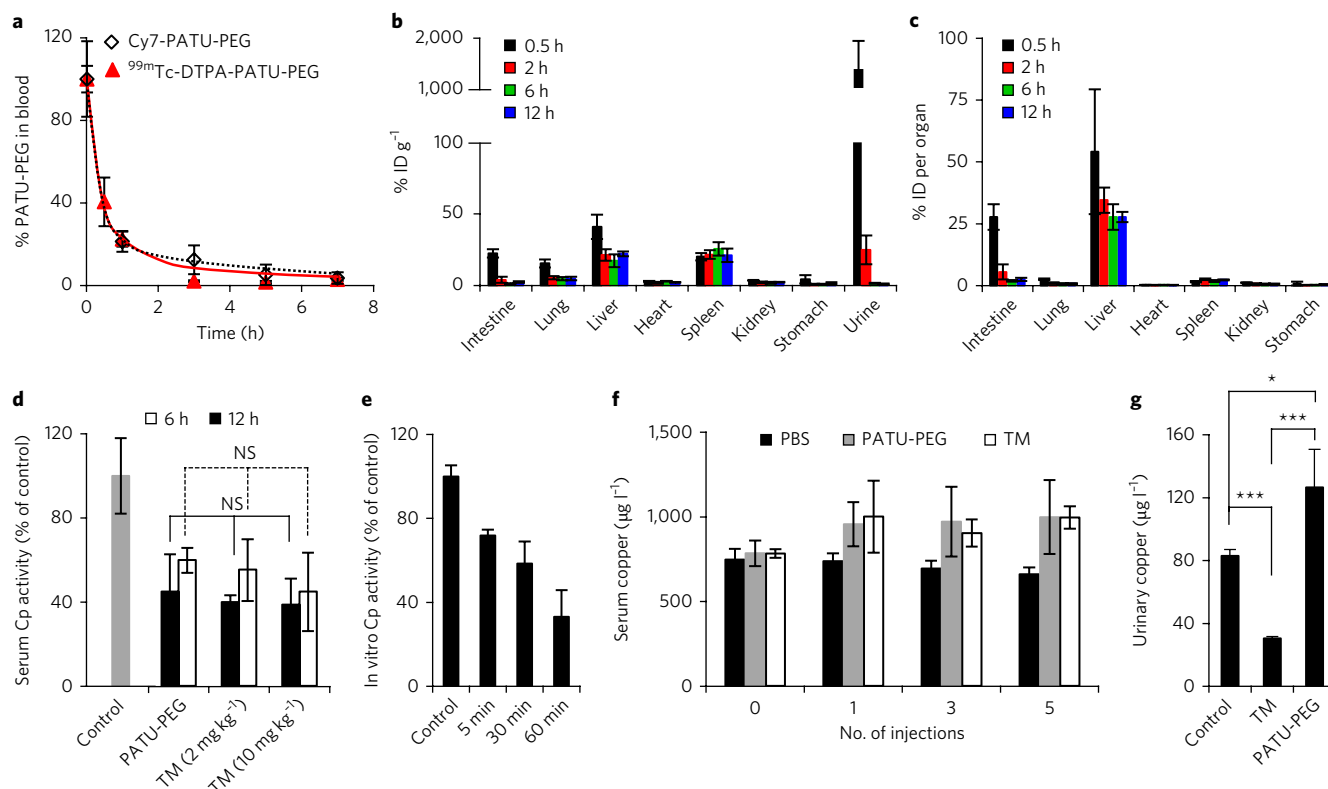


Fig. 7 | Preliminary pharmacological study of PATU-PEG. **a**, The plasma pharmacokinetic profiles of PATU-PEG determined by the fluorescence- or radio-labelling methods. Tumour-bearing nude mice ($n=3$) were intravenously injected with 50 mg kg^{-1} of either Cy7-PATU-PEG or $^{99\text{m}}\text{Tc-DTPA-PATU-PEG}$. The concentration in the plasma was normalized as the percentage of the injected dose (% PATU-PEG in plasma). **b, c**, Ex vivo biodistribution study of PATU-PEG. Mice ($n=3$ per time point) intravenously injected with Gd-DTPA-PATU-PEG (50 mg kg^{-1}) were killed after the indicated times and their urine and major organs were collected and analysed by ICP-MS. The PATU-PEG concentrations were normalized as the percentage of the injected dose (ID) per gram of each organ (% ID g^{-1} ; **b**) or per organ (% ID per organ; **c**). **d**, A dose titration for intravenously administered TM in terms of the reduced serum Cp activity in mice. Mice ($n=4\text{--}5$ per group) were intravenously injected with either TM (2 mg kg^{-1} or 10 mg kg^{-1}) or PATU-PEG (50 mg kg^{-1}). **e**, Effect of PATU-PEG on the oxidase activity of human Cp. Cp (300 mg l^{-1}) was co-incubated with PATU-PEG ($20 \text{ }\mu\text{M}$) in a sodium-free buffer at $37 \text{ }^\circ\text{C}$ for the indicated times, followed by Cp activity assay. **f**, Total serum copper concentrations in mice after treatments. Mice ($n=6$ per group) were intravenously injected with PBS, TM (2 mg kg^{-1}) or PATU-PEG (50 mg kg^{-1}) every other day for a total of five times. Blood samples were collected at 12 h post the indicated injection for serum copper measurements by ICP-MS. **g**, Urine copper levels after a single treatment. Mice ($n=4$ per group) were intravenously injected with PBS, TM (2 mg kg^{-1}) or PATU-PEG (50 mg kg^{-1}). Urine samples were collected within the first 4 h post injection for urinary copper measurements by ICP-MS. All data are expressed as mean \pm s.d. * $P < 0.05$; *** $P < 0.001$; NS, no significant difference.

rapid renal excretion of about 6–8 nm (ref. 48), this result indicates that a large fraction of the injected PATU-PEG was rapidly filtered into the urine. The fluorescence emission in the bladder disappeared gradually afterwards, whereas the fluorescence intensity in the liver did not change much. At 12 h post injection, the liver was the only organ with detectable fluorescence emission. No preferential accumulation in tumour site was observed, indicating that PATU-PEG was not tumour specific. The ex vivo results agreed well with the above in vivo observations (Supplementary Fig. 43b).

Furthermore, the ex vivo biodistribution studies using gadolinium-labelled PATU-PEG (Gd-DTAP-PATU-PEG) as the tracer allowed the accurate quantification of PATU-PEG in each organ (Fig. 7b). At 30 min post injection, the highest PATU-PEG concentration of $1,391.1 \pm 555.2\%$ injected dose per gram (ID g^{-1}) was found in the urine, and the second-highest was in the liver with $41.0 \pm 8.4\%$ ID g^{-1} , which agreed well with its aforementioned renal clearance. Also, the biodistribution study (Fig. 7c) showed that the remaining PATU-PEG was mostly sequestered into the liver ($27.7 \pm 5.2\%$ ID at 6 h); the uptake in other soft-tissue organs was negligible ($<1\%$ ID per organ after 6 h post injection).

Serum copper and Cp (a major copper transporter in blood) activity are currently the most widely used laboratory indicators to

evaluate copper status⁴⁹. Compared with the PBS treatment, a single i.v. injection of PATU-PEG at 50 mg kg^{-1} significantly lowered the Cp activity in mice, which is statistically equivalent to the levels after the TM treatments at i.v. doses of 2 mg kg^{-1} and 10 mg kg^{-1} (Fig. 7d). The ex vivo experiment proved that co-incubation of PATU-PEG with human Cp reduced the Cp activity in a time-dependent manner (Fig. 7e), indicating that PATU-PEG was indeed able to strip off copper from Cp. However, both the PATU-PEG and TM treatments slightly elevated the total serum copper levels in mice to a similar extent compared with the PBS treatment (Fig. 7f). In contrast, the urine samples of the PATU-PEG-treated mice contained 1.5 times more copper than the control (Fig. 7g). These results indicate that PATU-PEG complexed with bioavailable copper once intravenously administered; some of the complexes were filtrated through the kidney into urine while some were retained in the serum causing slight elevation of total serum copper. This is agreeable with the size of the PATU-PEG/Cu complex (about 9 nm and some even larger, Supplementary Figs. 24b and 25), which is larger than the renal filtration threshold (6–8 nm).

Other possible mechanisms involved in the anticancer activity of PATU-PEG were also explored. The possibility involving immunotherapy was first checked by measuring the change in serum

tumour necrosis factor- α (TNF- α), an important cytokine involved in immune response⁵⁰. The treatment with PATU-PEG did not affect the serum level of TNF- α (Supplementary Fig. 44), and the frequent treatments did not change the averaged weight of the spleens (Supplementary Fig. 45), suggesting no immunotherapy involved. Other tests showed that the PATU-PEG treatment also had no effects on the cancer stem cells (Supplementary Fig. 46) and autophagy (Supplementary Fig. 47). In addition, it was reported that acylthiourea and thiourea derivatives had potent Hedgehog (Hh) inhibiting activity⁵¹. Accordingly, we further checked the effects of PATU-PEG and PTU-PEG on the expression of Gli family zinc finger 1 (Gli1), the transcription factor of the Hh signalling, in Hh signalling-positive HepG2 tumour cells. The western blot analysis showed that PATU-PEG or PTU-PEG treatment did not induce significant change of Gli1 expression (Supplementary Fig. 48).

Discussion

Synthesis of dendrimers is generally very time consuming, and dendrimers that can be efficiently synthesized are very rare⁵². By the elaboration of two click reactions, isothiocyanate-amine coupling and thiol-methacrylate Michael addition, we designed two pairs of orthogonal monomers and synthesized PATU and PTU dendrimers (Fig. 1a,d) in a highly efficient way—growing one generation, including the reactions and purification/isolation, within 4 h with overall yields higher than 90%. Thus, grams of monodispersed G4 dendrimers could be prepared in a single day.

Interestingly, a very subtle difference between PATU and PTU dendrimers, with or without the acyl groups adjacent to the thiourea moieties, entitled them very different properties. In particular, PATU-PEG was significantly superior to PTU-PEG in anticancer activity (Fig. 4a and Supplementary Fig. 32b–f), indicating that the acylthioureas contribute better to the tumour inhibitory activity.

At a dose far below its LD₅₀ (50 versus >1,000 mg kg⁻¹; mice, i.v.), PATU-PEG effectively suppressed tumour growth with tumour inhibition ratios higher than 65% against multiple tumour models (Fig. 4). Furthermore, PATU-PEG not only effectively suppressed distant metastasis from primary tumours (Fig. 5a–d), leading to a great survival advantage, but also prevented circulating tumour cells from seeding in lungs (Fig. 6a–d). Because peripheral PEG is known to be biologically inert, it is reasonable to attribute the anticancer and anti-metastasis activities of PATU-PEG to its inner structural properties. Thus, the dendrimer itself, without any drug encapsulation or conjugation, is a macromolecular drug, unlike the current dendrimers that are used as inert carriers^{53–55}. It is also distinct from the previously so-called therapeutic dendrimers⁵⁶, which gain their bioactivities from their peripheral cationic²⁰, anionic¹⁷ or sugar groups⁵⁷.

Another equally important and interesting feature of PATU-PEG is its low toxicity. Cytotoxic chemotherapeutic agents inducing cell killing have been the main arsenal for cancer treatment. While only a small fraction of these administered drugs reaches tumour tissues to produce therapeutic effects, significant fractions inevitably distribute in healthy organs and thus intoxicate healthy cells, causing severe adverse effects, which is commonly responsible for dose limiting, low therapeutic efficacy and compromised quality of life of patients^{58–60}. PATU-PEG has low acute and subacute in vivo toxicity with an LD₅₀ (mice, i.v.) greater than 1,000 mg kg⁻¹ (Fig. 3). During the experiments, PATU-PEG did not cause any observable toxicity to animals even at high doses (e.g. 250 mg kg⁻¹) or more frequent dosing. This low toxicity profile of PATU-PEG also indicates that its innate anticancer mechanism is distinct from small-molecule acylthiourea or thiourea cytotoxins⁵¹.

The mechanisms underlying the tumour inhibitory behaviour of PATU-PEG were preliminarily investigated. Compared with healthy individuals, cancer patients have aberrantly elevated levels of serum and tumour copper⁶¹, which is recognized as a mandatory cofactor

for multiple proteins crucial for angiogenesis⁴², tumorigenesis⁶² and metastasis⁶³. Excessive copper influx promoted VEGF expression⁶⁴, increased microvessel counts in animals (Supplementary Fig. 38) and even led to animal death (Supplementary Fig. 36c). Copper depletion has been shown to suppress tumour angiogenesis and several pro-tumour pathways such as mitogen-activated protein kinase pathway⁶². Owing to the high copper-binding capability, PATU-PEG could sequester bioavailable copper resulting in in vivo copper depletion (Fig. 7d–g).

Accordingly, the high copper-chelation capability of PATU-PEG downregulated the VEGF expression (Fig. 4d and Supplementary Figs. 32c, 32d, 36f and S37) and neovascularization (Fig. 4d and Supplementary Figs. 32e and 36g) as well as the mitogen-activated protein kinase pathway (Supplementary Table 1), leading to tumour growth arrests (Fig. 4 and Supplementary Figs. 32b, 33, 36d, 39b, 40 and 41) as evidenced by the reduced Ki-67 expression (Fig. 4d and Supplementary Figs. 32c, 32f, 36h, 37a and 37e) and the promoted apoptosis (Fig. 4d).

Severe copper deficiency may lead to deficiencies in blood cells, bone and connective tissue abnormalities, and neurologic disorders^{65–68}. But the treatment of mice five times with PATU-PEG at the used dose of 50 mg kg⁻¹ for the anticancer experiments did not change the copper and zinc concentrations in main organs of the mice (Supplementary Fig. 49), alleviating the copper deficiency concern. It should be pointed out that the current available data did not involve the chronic use of PATU-PEG, and thus cannot show the chronic toxicity of PATU-PEG. Current research is underway to assess PATU-PEG's chronic toxicity.

PATU-PEG structures could be further optimized for better pharmacokinetics and biodistribution. The current PATU PEGylated with short PEG chains was only 3 nm in diameter, far smaller than the renal clearance threshold, and thus was quickly cleared by renal clearance, leading to low bioavailability (Fig. 7a–c). It can be expected that prolonging its circulation time and thus more effectively sequestering bioavailable copper would further enhance tumour accumulation and antitumour activity. Using higher generations of the PATU dendrimer or longer PEG chains will make the PATU-PEG size larger and thus prolong the circulation and further improve the pharmacokinetics and biodistribution. However, it is the PATU-PEG dendrimers excreted into the urine that contribute to the removal of bioavailable copper. Therefore, PATU-PEG should be further engineered to be able to circulate long enough in blood to sequester the copper but still have effective renal clearance.

This non-cytotoxic dendrimer with potent anticancer and anti-metastatic activities, along with its precise molecular structure and facile synthesis, may be developed as a new type of macromolecular anticancer agent. The exact anticancer mechanisms of PATU-PEG require further extensive study, and structural optimization is also needed for improved pharmacokinetics and thereby therapeutic efficacy. Furthermore, exerting bioactivity via stripping the copper from the body may also provide a new direction in drug discovery.

Methods

Cell lines. Human-origin lung adenocarcinoma (A549), breast carcinoma (BCap37 and MCF7), oral epidermoid carcinoma (KB), colorectal adenocarcinoma (SW620), ovarian carcinoma (SKOV3), cervical adenocarcinoma (HeLa), foetal lung fibroblast (HFL1) and immortalized human bronchial epithelial (BEAS-2B) cell lines were purchased from the American Type Culture Collection (Manassas). Human adriamycin resistant mammary carcinoma cell line (MCF7/ADR) was purchased from ACEA Biosciences. Mouse mammary adenocarcinoma stably expressing luciferase (Luc) and green fluorescent protein (GFP) cell line (4T1-Luc-GFP) was purchased from CellCyto. All cell lines have been tested for mycoplasma contamination, and authenticated by comparing the observed cellular morphologies with the reported ones.

A549, BCap37, SKOV3, MCF7, MCF7/ADR and 4T1-Luc-GFP cells were maintained in RPMI-1640 medium (Genom Biological Technology). KB, SW620, HeLa, J774 and HFL1 cells were grown in Dulbecco's modified Eagle's medium (DMEM) (Genom Biological Technology). BEAS-2B cells were grown in

DMEM/Ham's F-12 (1:1) (DF-12) (Genom Biological Technology). All culture media were supplemented with 10% heat-inactivated fetal bovine serum (Genom Biological Technology) and 1% penicillin/streptomycin. MCF7/ADR cells were maintained continuously with 0.5 μM of doxorubicin. All cell lines except SW620 were maintained in a humidified atmosphere of 5% CO_2 at 37°C. SW620 cells were cultured in a humidified atmosphere with no CO_2 . Subculturing of 80–90% confluent cells was routinely done using trypsin-EDTA solution (0.05% trypsin and 0.53 mmol l^{-1} EDTA).

On collection, cells were trypsinized and washed, then concentrated by centrifugation, and counted with a hemocytometer. The cells were assessed for viability (>95% viable) and then resuspended in PBS to a required density.

In vitro cytotoxicity assay. The cytotoxicity of PATU-PEG or PTU-PEG to tumour cell lines was determined by the MTT cell proliferation assay. Briefly, cells (~4,000–5,000 cells per well) were evenly plated into 96-well plates and grown to 70–80% confluence, followed by addition of PATU-PEG or PTU-PEG at set concentrations for 48 h. Subsequently, 20 μl MTT (5 mg ml^{-1}) in PBS was added to each well and incubated at 37°C for 3 h to allow for complete cleavage of the tetrazolium salt by metabolically active cells. Finally, the medium containing MTT was removed and 100 μl DMSO was added to each well. The absorbance in each individual well was determined at 562 nm using the Molecular Devices microplate reader. Each drug concentration was tested in triplicate and in three independent experiments.

Colony formation assay. Cells (~200–400 cells per well) seeded in a six-well culture plate were treated with or without PATU-PEG (200 $\mu\text{g ml}^{-1}$). After culture for 10 d, cells were carefully washed with PBS twice, fixed with methanol and stained with crystal violet for colony visualization and counting. Colonies with more than 50 cells were counted. Three independent experiments were performed.

Animal maintenance. All animal uses were approved by the Animal Care and Use Committee of Zhejiang University. Mice were purchased from Zhejiang University Animal Center and housed in sterile cages of five animals or less within laminar airflow hoods in a specific pathogen-free room with a 12 h light/12 h dark schedule and fed autoclaved chow and water ad libitum. In general, mice were used for experiments after acclimation for one week.

Acute toxicity assessment. The acute toxicity of PATU-PEG was studied using ICR strain mice with an initial body weight of ~18–21 g. Mice were randomly divided into five groups of ten (five males and five females) and maintained under the standard conditions with free access to food and water. After one-week acclimation, PATU-PEG in 0.2 ml of sterile PBS was injected via the tail vein at doses of 1914.1, 1531.3, 1225.0, 980.0 and 784.0 mg kg^{-1} , respectively. Animals were observed every 1–2 h on the treatment day, twice a day later, for up to 14 d post injection. The intoxication symptoms, changes in body weight and the time of death of the treated mice were recorded in detail. The LD_{50} and 95% confidence interval were calculated by the Bliss method.

Serum chemistry. ICR mice were intravenously injected with PBS or PATU-PEG (50 mg kg^{-1} or 100 mg kg^{-1}) daily for 5 d. Blood samples were collected for serum chemistry analysis one day after the fifth injection. Alanine transaminase, creatine kinase, creatine kinase mb isoenzyme, aspartate transaminase, lactate dehydrogenase, blood urea nitrogen and creatinine were measured in serum using the Johnson & Johnson Vitros 5600 Integrated System (Ortho-Clinical Diagnostics). All data are expressed as mean \pm s.d.

Human xenograft tumour model. Six- to eight-week-old female BALB/c homozygous athymic nude mice were inoculated with BCaP37 (1×10^6 per mouse), SW620 (3×10^6 cells per mouse), or MCF7/ADR (7×10^6 cells per mouse) via subcutaneous (s.c.) injection to the right flank using 1.5 inch (38.1 mm), 27-gauge needles. The animals were randomized and the treatments were started after ~5–7 d post inoculation. Tumour volume (mm^3) was calculated using the formula $V (\text{mm}^3) = L (\text{mm}) \times W (\text{mm})^2 \times 0.5$, where L and W were the longest and widest diameters of a tumour. At the end of the experiments, animals were killed according to the regulations of the Animal Care and Use Committee of Zhejiang University. Tumours were resected, weighed and fixed in 10% neutral-buffered formalin for paraffin embedding. The inhibition ratio of tumour growth was calculated using the following formula: inhibition ratio = (mean tumour weight of the control group – mean tumour weight of the experimental group) / mean tumour weight of the control group \times 100%.

Murine mammary carcinoma metastasis model. 4T1-Luc-GFP cells (2×10^5 cells per mouse) suspended in 200 μl PBS were inoculated subcutaneously into the right hind leg of six- to eight-week-old syngeneic female BALB/c mice. They were randomized and tagged. The treatments were started after 7 d post inoculation. The s.c. tumours were measured as indicated. Tumour metastasis was detected by quantitative bioluminescence imaging. For the bioluminescence imaging, animals were injected intraperitoneally with D-luciferin sodium salt (Gold Biotechnology) at 150 mg kg^{-1} body weight in 0.2 ml PBS. After 10 min,

the animals were imaged (60 s exposure per image) under anaesthesia with 2.5% isoflurane using a Xenogen IVIS Lumina system (Caliper Life Sciences). Acquired images were obtained by superimposing the emitted light over the greyscale photographs of the animals. Quantitative analysis was done with Lumina II Living Image 4.2 software.

For the lung metastasis model, 4T1-Luc-GFP cells (2×10^5 cells per mouse) were intravenously injected into mice via the tail vein. The treatments were started after 1 d post-injection. Bioluminescence imaging was carried out on the tenth day post injection.

In accordance with Zhejiang University animal use protocols, animals used for the metastasis models were killed at earlier time points if signs of morbidity were observed. All animals that survived at experimental endpoints were euthanized. For the lung metastasis model, animals were killed after the in vivo imaging. Lungs were retrieved for histological examination and visual counting of pulmonary nodules.

Histology and immunohistochemistry. Tissue specimens were fixed in 10% neutral-buffered formalin and embedded in paraffin. Sections of 4 μm thickness were stained with haematoxylin and eosin (H&E) or used for immunohistochemical studies. For immunohistochemistry, sections were deparaffinized, rehydrated and subjected to epitope retrieval and stained with primary antibodies for 24 h at 4°C, reacted with horseradish peroxidase (HRP)-conjugated secondary antibody for 1 h, and diaminobenzidine (DAB) was used as the substrate to produce an observable brown colour. The following primary antibodies were used: rabbit anti-CD31 (cat. # ZA-0568, ZSGB-Bio OriGene), mouse anti-Ki67 (cat. # TA500265, ZSGB-Bio OriGene) and rabbit anti-VEGF (cat. # sc-152, Santa Cruz). Apoptotic events were determined by the TUNEL assay. Sections were subjected to TUNEL staining using an In Situ Cell Death Detection Kit, POD according to the manufacturer's protocol (Roche). Apoptotic cells were identified by positive TUNEL staining. Negative controls were carried out by omitting the primary antibodies and substituting the primary antibody with antibody diluent. Pictures were taken using an Olympus BX61 upright microscope equipped with an Olympus DP26 charge-coupled device camera. Ki-67 analysis was based on the use of ImageJ 1.47v (Wayne Rasband, National Institutes of Health) and Ki-67 labelling index was calculated by dividing the DAB staining area by the total nuclear area in six random $\times 400$ fields. To evaluate VEGF expression, five random $\times 400$ fields from each specimen were observed and a scoring method according to Volm's method⁶⁹ was established corresponding to the sum of: (1) the percentage of positive cells (0, 0% positive cells; 1, 25% positive cells; 2, 26–50% positive cells; and 3, >50% positive cells); and (2) the staining intensity (0, negative; 1, weak; 2, moderate; 3, high). A single countable microvessel was defined as any CD31-staining endothelial cell or endothelial-cell cluster that was clearly separate from adjacent microvessels, tumour cells and other connective-tissue elements⁷⁰. Vessel lumens or red cells, although usually present, were not necessary for a structure to be defined as a microvessel. To assess microvessel density, the total number of stained vessels was determined in five random $\times 400$ fields. All the results were reported in a blinded fashion for each tumour.

Histological fluorescence and confocal microscopy. Tissues were fixed overnight in paraformaldehyde, and cryoembedded in the Jung Tissue Freezing Medium (Leica Microsystems). Sections of 10 μm thickness were cut by a cryostat (Leica CM1950; Leica Microsystems) and stained with 4',6-diamidino-2-phenylindole (DAPI). GFP positive cells were detected by their intrinsic signal. Fluorescence images were obtained using the Nikon-A1 confocal laser scanning microscope system (CLSM; Nikon).

Plasma pharmacokinetics of PATU-PEG in tumour-bearing mice. Both Cy7-PATU-PEG and ^{99m}Tc-DTPA-PATU-PEG were employed for the plasma pharmacokinetics study of PATU-PEG.

For the fluorescence-based method, Cy7-PATU-PEG (50 mg kg^{-1}) was intravenously injected through the tail vein into MCF7/ADR tumour-bearing nude mice ($n = 3$). Blood samples (~100 μl) were then collected via the orbital venous plexus of mice at 0.017, 1, 3, 5 and 7 h post injection. Plasma was separated from the whole blood by centrifuging at 2,408g for 10 min. The fluorescence intensity of Cy7 was measured at an emission wavelength of 790 nm excited at 760 nm using the Molecular Devices microplate reader. Blank blood samples were measured to determine the blood autofluorescence level at this wavelength range.

In the case of ^{99m}Tc-DTPA-PATU-PEG, each nude mouse bearing BCaP37 xenograft was intravenously injected with 50 mg kg^{-1} of ^{99m}Tc-DTPA-PATU-PEG (0.40 mCi). Blood samples (~20 μl) were then collected at 0.017, 0.5, 1, 3, 5 and 7 h post injection, and weighed, respectively. Radioactivity in the blood samples was counted in the GC-1500 gamma counter (USTC Chuangxin) and calibrated against a known aliquot of the original injectate counted at the same time.

At the experimental endpoint, animals were killed in accordance with the regulations of the Animal Care and Use Committee of Zhejiang University.

Biodistribution of PATU-PEG in mice. Nude mice bearing MCF7/ADR xenografts were intravenously injected with Cy7-PATU-PEG (50 mg kg^{-1})

and then imaged (120 s exposure per image) under anaesthesia with 1% sodium pentobarbital at 0.5, 1, 2, 6 and 12 h post injection using a Kodak In-Vivo FX Professional Imaging System (Kodak). Two mice were killed at 0.5 or 12 h post injection. Tumours and major organs, including liver, heart, spleen, kidney, stomach and lung, were immediately dissected, washed with PBS and the fluorescence images were obtained. The fluorescence in vivo and ex vivo was detected at excitation and emission wavelengths of 760 nm and 790 nm, respectively.

To validate the results obtained by the fluorescence-based method, mice were intravenously injected with Gd-DTPA-PATU-PEG at a dose of 50 mg kg⁻¹, and then killed at 0.5, 2, 6 and 12 h post injection. The urine and major organs, including intestine, lung, liver, heart, spleen, kidney and stomach were collected and weighed. The organ samples were digested with ultra-pure nitric acid, and the obtained solutions were calibrated to give a volume of 5 ml by adding ultra-pure water. Urine samples (20 µl per mouse) were mixed with nitric acid and diluted to a volume of 5 ml. The Gd concentrations in these solutions and the original injectate were measured by inductively coupled plasma mass spectrometry (ICP-MS). The percentages of injected dose per gram of organ (% ID g⁻¹) and per organ (% ID per organ) were calculated by comparing the concentrations in samples with that of the ID.

Cp activity assay. Serum Cp was assayed based on its oxidase activity using the standard method^{71,72}. Briefly, blood samples were collected in tubes from the retrobulbar venous plexus of mice. Blood samples, averaging ~100–200 µl per mouse, were centrifuged at 4,720g for 2 min (4 °C). Two tubes each containing 50 µl mouse serum and 750 µl of 0.1 M sodium acetate buffer (pH 5.0) were incubated for 5 min in a 30 °C water bath. Pre-warmed 200 µl *o*-dianisidine dihydrochloride solution (2.5 g l⁻¹, 7.88 mM; Sigma) was then added into each tube. The reactions were allowed to continue for exactly 30 min in one tube and exactly 45 min in the other one. Finally, the reactions were terminated by adding 2 ml of 9 M sulfuric acid. The absorbance of both tubes was measured at 540 nm using the Molecular Devices microplate reader. Cp activity in IU was calculated using the formula Cp oxidase activity = $(A_{45} - A_{30}) \times 0.625 \text{ U mL}^{-1}$, where A_{45} and A_{30} are the absorbance at 45 and 30 min, respectively.

In vitro effect of PATU-PEG on Cp activity. Human Cp (300 mg l⁻¹; Athens Research and Technology) was co-incubated with PATU-PEG (20 µM) in a sodium-free buffer (50 mM potassium phosphate, pH 6.8, with 100 mM KCl, 20 mM ϵ -amino-*n*-caproic acid and 5 mM ethylenediaminetetraacetic acid) at 37 °C for 5 min, 30 min and 60 min, followed by Cp activity assay.

Urinary copper measurements. Urine samples of mice were collected in tubes by bladder puncture. Urine (200 µl per mouse) was digested in ultra-pure nitric acid and the obtained solution was fixed to a volume of 2 ml with ultra-pure water. Cobalt (100 parts per 10⁹) was added to each sample as an internal control for ICP-MS analysis.

Serum copper measurements. Blood samples collected from the retrobulbar venous plexus of mice, averaging ~100–200 µl per mouse, were centrifuged at 4,720g for 2 min (4 °C). Serum (50 µl per mouse) was collected and digested in ultra-pure nitric acid. The obtained solution was diluted to a volume of 4 ml with ultra-pure water and subjected to ICP-MS analysis of copper concentration.

Statistical analysis. Data analysis was carried out using SPSS 16.0 (SPSS). For multiple comparisons, one-way analysis of variance followed by a Tukey post-hoc test was performed. For individual comparisons, a two-tailed, unpaired Student's *t*-test was performed. All data are presented as mean \pm s.d. *P* < 0.05 was considered statistically significant.

Data availability. All data generated or analysed during this study are included in this article (and its Supplementary Information), and are available from the corresponding author on reasonable request.

Received: 26 September 2016; Accepted: 1 August 2017;

References

- Kolate, A. et al. PEG—a versatile conjugating ligand for drugs and drug delivery systems. *J. Control. Release* **192**, 67–81 (2014).
- Kopeček, J. Polymer–drug conjugates: origins, progress to date and future directions. *Adv. Drug Del. Rev.* **65**, 49–59 (2013).
- Zelikin, A. N., Ehrhardt, C. & Healy, A. M. Materials and methods for delivery of biological drugs. *Nat. Chem.* **8**, 997–1007 (2016).
- Cabral, H. & Kataoka, K. Progress of drug-loaded polymeric micelles into clinical studies. *J. Control. Release* **190**, 465–476 (2014).
- Shi, J. J., Kantoff, P. W., Wooster, R. & Farokhzad, O. C. Cancer nanomedicine: progress, challenges and opportunities. *Nat. Rev. Cancer* **17**, 20–37 (2017).
- Werle, M. Natural and synthetic polymers as inhibitors of drug efflux pumps. *Pharm. Res.* **25**, 500–511 (2008).
- Sosnik, A. Reversal of multidrug resistance by the inhibition of ATP-binding cassette pumps employing “Generally Recognized As Safe” (GRAS) nanopharmaceuticals: a review. *Adv. Drug Del. Rev.* **65**, 1828–1851 (2013).
- Alakhova, D. Y. & Kabanov, A. V. Pluronic and MDR reversal: an update. *Mol. Pharm.* **11**, 2566–2578 (2014).
- Thota, B. N. S., Urner, L. H. & Haag, R. Supramolecular architectures of dendritic amphiphiles in water. *Chem. Rev.* **116**, 2079–2102 (2016).
- Hsu, H.-J., Bugno, J., Lee, S.-R. & Hong, S. Dendrimer-based nanocarriers: a versatile platform for drug delivery. *Wiley. Interdiscip. Rev. Nanomed. Nanobiotechnol.* **9**, e1409 (2017).
- Khandare, J., Calderon, M., Dagia, N. M. & Haag, R. Multifunctional dendritic polymers in nanomedicine: opportunities and challenges. *Chem. Soc. Rev.* **41**, 2824–2848 (2012).
- Wei, T. et al. Anticancer drug nanomicelles formed by self-assembling amphiphilic dendrimer to combat cancer drug resistance. *Proc. Natl Acad. Sci. USA* **112**, 2978–2983 (2015).
- Chauhan, A. S., Diwan, P. V., Jain, N. K. & Tomalia, D. A. Unexpected in vivo anti-inflammatory activity observed for simple, surface functionalized poly(amidoamine) dendrimers. *Biomacromolecules* **10**, 1195–1202 (2009).
- Dernedde, J. et al. Dendritic polyglycerol sulfates as multivalent inhibitors of inflammation. *Proc. Natl Acad. Sci. USA* **107**, 19679–19684 (2010).
- Rele, S. M. et al. Dendrimer-like PEO glycopolymers exhibit anti-inflammatory properties. *J. Am. Chem. Soc.* **127**, 10132–10133 (2005).
- Portevin, D. et al. Regulatory activity of azabisphosphonate-capped dendrimers on human CD4⁺ T cell proliferation enhances ex-vivo expansion of NK cells from PBMCs for immunotherapy. *J. Transl. Med.* **7**, 82 (2009).
- Hayder, M. et al. A phosphorus-based dendrimer targets inflammation and osteoclastogenesis in experimental arthritis. *Sci. Transl. Med.* **3**, 81ra35 (2011).
- Price, C. F. et al. SPL7013 Gel (VivaGel®) retains potent HIV-1 and HSV-2 inhibitory activity following vaginal administration in humans. *PLoS ONE* **6**, e24095 (2011).
- Dufès, C. et al. Synthetic anticancer gene medicine exploits intrinsic antitumor activity of cationic vector to cure established tumors. *Cancer Res.* **65**, 8079–8084 (2005).
- Al-Jamal, K. T. et al. Systemic antiangiogenic activity of cationic poly-L-lysine dendrimer delays tumor growth. *Proc. Natl Acad. Sci. USA* **107**, 3966–3971 (2010).
- Ciepluch, K. et al. Biological properties of new viologen-phosphorus dendrimers. *Mol. Pharm.* **9**, 448–457 (2012).
- Abdel-Rahman, M. A. & Al-Abd, A. M. Thermoresponsive dendrimers based on oligoethylene glycols: design, synthesis and cytotoxic activity against MCF-7 breast cancer cells. *Eur. J. Med. Chem.* **69**, 848–854 (2013).
- Sliwkowski, M. X. & Mellman, I. Antibody therapeutics in cancer. *Science* **341**, 1192–1198 (2013).
- Scott, A. M., Wolchok, J. D. & Old, L. J. Antibody therapy of cancer. *Nat. Rev. Cancer* **12**, 278–287 (2012).
- Duncan, R. Polymer therapeutics: top 10 selling pharmaceuticals—What next? *J. Control. Release* **190**, 371–380 (2014).
- Maeda, H., Nakamura, H. & Fang, J. The EPR effect for macromolecular drug delivery to solid tumors: improvement of tumor uptake, lowering of systemic toxicity, and distinct tumor imaging in vivo. *Adv. Drug Del. Rev.* **65**, 71–79 (2013).
- Dubacheva, G. V. et al. Superselective targeting using multivalent polymers. *J. Am. Chem. Soc.* **136**, 1722–1725 (2014).
- Tito, N. B. & Frenkel, D. Optimizing the selectivity of surface-adsorbing multivalent polymers. *Macromolecules* **47**, 7496–7509 (2014).
- Zhang, W. et al. Redox-hypersensitive organic nanoparticles for selective treatment of cancer cells. *Chem. Mater.* **28**, 4440–4446 (2016).
- Barner-Kowollik, C. et al. “Clicking” polymers or just efficient linking: What is the difference? *Angew. Chem. Int. Ed.* **50**, 60–62 (2011).
- Xiao, S., Turkyilmaz, S. & Smith, B. D. Convenient synthesis of multivalent zinc(II)-dipicolylamine complexes for molecular recognition. *Tetrahedron Lett.* **54**, 861–864 (2013).
- Nair, D. P. et al. The thiol-Michael addition click reaction: a powerful and widely used tool in materials chemistry. *Chem. Mater.* **26**, 724–744 (2014).
- Restani, R. B. et al. Biocompatible polyurea dendrimers with pH-dependent fluorescence. *Angew. Chem. Int. Ed.* **51**, 5162–5165 (2012).
- Wang, D., Imae, T. & Miki, M. Fluorescence emission from PAMAM and PPI dendrimers. *J. Colloid Interface Sci.* **306**, 222–227 (2007).
- Wang, H., Zhao, E., Lam, J. W. Y. & Tang, B. Z. AIE luminogens: emission brightened by aggregation. *Mater. Today* **18**, 365–377 (2015).
- Zhang Yuan, W. & Zhang, Y. Nonconventional macromolecular luminogens with aggregation-induced emission characteristics. *J. Polym. Sci. A Polym. Chem.* **55**, 560–574 (2017).

37. Hu, R., Leung, N. L. & Tang, B. Z. AIE macromolecules: syntheses, structures and functionalities. *Chem. Soc. Rev.* **43**, 4494–4562 (2014).
38. Shen, Y. et al. Multifunctioning pH-responsive nanoparticles from hierarchical self-assembly of polymer brush for cancer drug delivery. *AIChE J.* **54**, 2979–2989 (2008).
39. Krzewska, S., Pajdowski, L. & Podsiadly, H. Studies on the reaction of copper (II) with thiourea-II: the modification of Bjerrum's method. The determination of equilibrium in simultaneous redox and complexation reactions. *J. Inorg. Nucl. Chem.* **42**, 87–88 (1980).
40. Campos, C., Guzmán, R., López-Fernández, E. & Casado, Á. Evaluation of the copper(II) reduction assay using bathocuproinedisulfonic acid disodium salt for the total antioxidant capacity assessment: the CUPRAC–BCS assay. *Anal. Biochem.* **392**, 37–44 (2009).
41. El Brahmī, N. et al. Original multivalent copper(II)-conjugated phosphorus dendrimers and corresponding mononuclear copper(II) complexes with antitumoral activities. *Mol. Pharm.* **10**, 1459–1464 (2013).
42. Jain, S. et al. Tetrathiomolybdate-associated copper depletion decreases circulating endothelial progenitor cells in women with breast cancer at high risk of relapse. *Ann. Oncol.* **24**, 1491–1498 (2013).
43. Sun, Q. et al. Integration of nanoassembly functions for an effective delivery cascade for cancer drugs. *Adv. Mater.* **26**, 7615–7621 (2014).
44. Chen, L. et al. Rejection of metastatic 4T1 breast cancer by attenuation of Treg cells in combination with immune stimulation. *Mol. Ther.* **15**, 2194–2202 (2007).
45. Larive, R. M. et al. Contribution of the R-Ras2 GTP-binding protein to primary breast tumorigenesis and late-stage metastatic disease. *Nat. Commun.* **5**, 3881 (2014).
46. Hua, K.-T. et al. N- α -Acetyltransferase 10 protein suppresses cancer cell metastasis by binding PIX proteins and inhibiting Cdc42/Rac1 activity. *Cancer Cell* **19**, 218–231 (2011).
47. Gao, D. et al. Endothelial progenitor cells control the angiogenic switch in mouse lung metastasis. *Science* **319**, 195–198 (2008).
48. Longmire, M., Choyke, P. L. & Kobayashi, H. Clearance properties of nano-sized particles and molecules as imaging agents: considerations and caveats. *Nanomedicine* **3**, 703–717 (2008).
49. Olivares, M., Méndez, M. A., Astudillo, P. A. & Pizarro, F. Present situation of biomarkers for copper status. *Am. J. Clin. Nutr.* **88**, 859S–862S (2008).
50. Kalliolias, G. D. & Ivashkiv, L. B. TNF biology, pathogenic mechanisms and emerging therapeutic strategies. *Nat. Rev. Rheumatol.* **12**, 49–62 (2016).
51. Solinas, A. et al. Acylthiourea, acylurea, and acylguanidine derivatives with potent Hedgehog inhibiting activity. *J. Med. Chem.* **55**, 1559–1571 (2012).
52. Antoni, P. et al. Pushing the limits for thiol-ene and CuAAC reactions: synthesis of a 6th generation dendrimer in a single day. *Macromolecules* **43**, 6625–6631 (2010).
53. Lee, C. C., MacKay, J. A., Frechet, J. M. J. & Szoka, F. C. Designing dendrimers for biological applications. *Nat. Biotechnol.* **23**, 1517–1526 (2005).
54. Kesharwani, P., Jain, K. & Jain, N. K. Dendrimer as nanocarrier for drug delivery. *Prog. Polym. Sci.* **39**, 268–307 (2014).
55. Liu, X. X. et al. Adaptive amphiphilic dendrimer-based nanoassemblies as robust and versatile siRNA delivery systems. *Angew. Chem. Int. Ed.* **53**, 11822–11827 (2014).
56. Ornelas, C. Brief timeline on dendrimer chemistry: advances, limitations, and expectations. *Macromol. Chem. Phys.* **217**, 149–174 (2016).
57. Shaunak, S. et al. Polyvalent dendrimer glucosamine conjugates prevent scar tissue formation. *Nat. Biotechnol.* **22**, 977–984 (2004).
58. Lipshultz, S. E., Cochran, T. R., Franco, V. I. & Miller, T. L. Treatment-related cardiotoxicity in survivors of childhood cancer. *Nat. Rev. Clin. Oncol.* **10**, 697–710 (2013).
59. Sahni, V., Choudhury, D. & Ahmed, Z. Chemotherapy-associated renal dysfunction. *Nat. Rev. Nephrol.* **5**, 450–462 (2009).
60. Schiff, D., Wen, P. Y. & van den Bent, M. J. Neurological adverse effects caused by cytotoxic and targeted therapies. *Nat. Rev. Clin. Oncol.* **6**, 596–603 (2009).
61. Gupte, A. & Mumper, R. J. Elevated copper and oxidative stress in cancer cells as a target for cancer treatment. *Cancer Treat. Rev.* **35**, 32–46 (2009).
62. Brady, D. C. et al. Copper is required for oncogenic BRAF signalling and tumorigenesis. *Nature* **509**, 492–496 (2014).
63. MacDonald, G. et al. Memo is a copper-dependent redox protein with an essential role in migration and metastasis. *Sci. Signal.* **7**, ra56 (2014).
64. Martin, F. et al. Copper-dependent activation of hypoxia-inducible factor (HIF)-1: implications for ceruloplasmin regulation. *Blood* **105**, 4613–4619 (2005).
65. Lazarchick, J. Update on anemia and neutropenia in copper deficiency. *Curr. Opin. Hematol.* **19**, 58–60 (2012).
66. Madsen, E. & Gitlin, J. D. Copper deficiency. *Curr. Opin. Gastroenterol.* **23**, 187–192 (2007).
67. Klevay, L. M. Cardiovascular disease from copper deficiency—a history. *J. Nutr.* **130**, 489S–492S (2000).
68. Olivares, M. & Uauy, R. Copper as an essential nutrient. *Am. J. Clin. Nutr.* **63**, 791S–796S (1996).
69. Volm, M., Koomägi, R. & Mattern, J. Prognostic value of vascular endothelial growth factor and its receptor Flt-1 in squamous cell lung cancer. *Int. J. Cancer* **74**, 64–68 (1997).
70. Weidner, N., Semple, J. P., Welch, W. R. & Folkman, J. Tumor angiogenesis and metastasis—correlation in invasive breast carcinoma. *N. Engl. J. Med.* **324**, 1–8 (1991).
71. Hassouneh, B. et al. Tetrathiomolybdate promotes tumor necrosis and prevents distant metastases by suppressing angiogenesis in head and neck cancer. *Mol. Cancer Ther.* **6**, 1039–1045 (2007).
72. Schosinsky, K. H., Lehmann, H. P. & Beeler, M. F. Measurement of ceruloplasmin from its oxidase activity in serum by use of *o*-dianisidine dihydrochloride. *Clin. Chem.* **20**, 1556–1563 (1974).

Acknowledgements

We thank the National Basic Research Program of China (2014CB931900), the National Natural Science Foundation of China (51390481, U1501243, 51522304, 21090352 and 50888001) and the Doctoral Fund of Ministry of Education of China (20110101130007) for financial support.

Author contributions

Y.S. designed and supervised the project and wrote the manuscript with S.S.; S.S., Q.Z. and J.S. carried out all the experiments; M.W. checked the anticancer activity; X.L., J.G., R.X. and K.W. instructed the bioassays; J.T. instructed the synthesis.

Competing interests

The authors declare no competing financial interests.

Additional information

Supplementary information is available for this paper at doi:10.1038/s41551-017-0130-9.

Reprints and permissions information is available at www.nature.com/reprints.

Correspondence and requests for materials should be addressed to Y.S.

Publisher's note: Springer Nature remains neutral with regard to jurisdictional claims in published maps and institutional affiliations.

Life Sciences Reporting Summary

Nature Research wishes to improve the reproducibility of the work that we publish. This form is intended for publication with all accepted life science papers and provides structure for consistency and transparency in reporting. Every life science submission will use this form; some list items might not apply to an individual manuscript, but all fields must be completed for clarity.

For further information on the points included in this form, see [Reporting Life Sciences Research](#). For further information on Nature Research policies, including our [data availability policy](#), see [Authors & Referees](#) and the [Editorial Policy Checklist](#).

▶ Experimental design

1. Sample size

Describe how sample size was determined.

The sample sizes (mostly, the number of mice per group in the anticancer experiments) are indicated in the manuscript. The sample size follows the standard of the animal uses.

2. Data exclusions

Describe any data exclusions.

No data were excluded.

3. Replication

Describe whether the experimental findings were reliably reproduced.

Yes. Particularly, the anticancer activity experiments were repeated by two persons in the same (Shen's lab) and checked by another person in Gao's lab in the Pharmacy Department.

4. Randomization

Describe how samples/organisms/participants were allocated into experimental groups.

The mice were grouped randomly; One of the participants (Shao) was the original discover and did part of the experiment; Zhou did the rest experiments after Shao graduated; M. Wang redid some experiments for validation. The number of mice per group was determined as described in #3.

5. Blinding

Describe whether the investigators were blinded to group allocation during data collection and/or analysis.

At the most time, the investigators were aware of the group allocation. But for immunohistochemical analysis, the investigators were blinded to the group allocation.

Note: all studies involving animals and/or human research participants must disclose whether blinding and randomization were used.

6. Statistical parameters

For all figures and tables that use statistical methods, confirm that the following items are present in relevant figure legends (or in the Methods section if additional space is needed).

n/a Confirmed

- The exact sample size (n) for each experimental group/condition, given as a discrete number and unit of measurement (animals, litters, cultures, etc.)
- A description of how samples were collected, noting whether measurements were taken from distinct samples or whether the same sample was measured repeatedly
- A statement indicating how many times each experiment was replicated
- The statistical test(s) used and whether they are one- or two-sided (note: only common tests should be described solely by name; more complex techniques should be described in the Methods section)
- A description of any assumptions or corrections, such as an adjustment for multiple comparisons
- The test results (e.g. P values) given as exact values whenever possible and with confidence intervals noted
- A clear description of statistics including central tendency (e.g. median, mean) and variation (e.g. standard deviation, interquartile range)
- Clearly defined error bars

See the web collection on [statistics for biologists](#) for further resources and guidance.

► Software

Policy information about [availability of computer code](#)

7. Software

Describe the software used to analyze the data in this study.

SPSS, MS Excel

For manuscripts utilizing custom algorithms or software that are central to the paper but not yet described in the published literature, software must be made available to editors and reviewers upon request. We strongly encourage code deposition in a community repository (e.g. GitHub). *Nature Methods* [guidance for providing algorithms and software for publication](#) provides further information on this topic.

► Materials and reagents

Policy information about [availability of materials](#)

8. Materials availability

Indicate whether there are restrictions on availability of unique materials or if these materials are only available for distribution by a for-profit company.

There are no restrictions on materials availability.

9. Antibodies

Describe the antibodies used and how they were validated for use in the system under study (i.e. assay and species).

Rabbit anti-CD31, mouse anti-Ki67, rabbit anti-VEGF, anti-Gli1, anti-tubulin, anti-human CD24-PE and CD44-FITC antibodies. They were validated by positive controls.

10. Eukaryotic cell lines

a. State the source of each eukaryotic cell line used.

Human-origin lung adenocarcinoma (A549), breast carcinoma (BCap37 and MCF7), oral epidermoid carcinoma (KB), colorectal adenocarcinoma (SW620), ovarian carcinoma (SKOV3), cervical adenocarcinoma (Hela), foetal lung fibroblast (HFL1), immortalized human bronchial epithelial (BEAS-2B) cell lines were purchased from the American Type Culture Collection (Manassas, USA). Human adriamycin resistant mammary carcinoma cell line (MCF7/ADR) was purchased from ACEA Biosciences Inc. (Hangzhou, China). Mouse mammary adenocarcinoma stably expressing luciferase (Luc) and green fluorescent protein (GFP) cell line (4T1-Luc-GFP) was purchased from CellCyto Inc. (Beijing, China).

b. Describe the method of cell line authentication used.

By comparing the observed cellular morphology with the reported one.

c. Report whether the cell lines were tested for mycoplasma contamination.

Yes.

d. If any of the cell lines used are listed in the database of commonly misidentified cell lines maintained by [ICLAC](#), provide a scientific rationale for their use.

KB and MCF7/ADR cell lines are listed. We checked that the MCF7/ADR cells were indeed very resistant to DOX. Thus, we just used it for checking the bioactivity of these two dendrimers to DOX-resistant cells. KB cells were used to test tumor specificity with other cell lines.

► Animals and human research participants

Policy information about [studies involving animals](#); when reporting animal research, follow the [ARRIVE guidelines](#)

11. Description of research animals

Provide details on animals and/or animal-derived materials used in the study.

BALB/c mice, ICR mice and BLAB/c nude mice.

Policy information about [studies involving human research participants](#)

12. Description of human research participants

Describe the covariate-relevant population characteristics of the human research participants.

No human research participants were involved.